Overview of plasma diagnostics (high energy density plasmas)

S.V. Lebedev

Imperial College London

General comments

HEDP systems *emit*:
- **Visible, XUV, x-ray photons**
- **Charged particles**
- **Neutrons**

Can be *probed* by similar particles

Small objects – high spatial and temporal resolution (10μm, 1ns)

Principles of plasma diagnostics are mostly common for all types of plasmas

s.lebedev@ic.ac.uk

Outline

Electrical measurements: magnetic field and current

Laser probing: interferometry, density gradients

Emission: spectral lines, continuum

Thomson scattering

X-ray imaging

Proton probing

s.lebedev@ic.ac.uk

Magnetic field

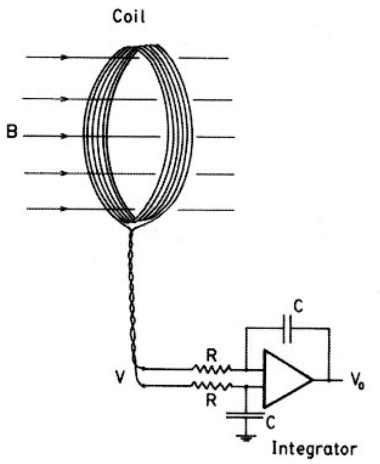

Magnetic coil

$$\oint_C \vec{E}\cdot d\vec{l} = -\iint_S \dot{\vec{B}}\cdot d\vec{s} \qquad V = NA\dot{B}$$

after integrator: $$\boxed{B(t) = \frac{RC}{NA}\cdot V_{\text{int}}(t)}$$

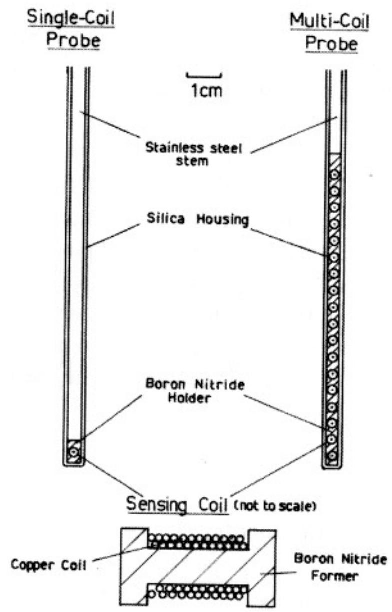

Example of magnetic probe designed to measure magnetic field distribution inside the plasma

More often a set of coils outside

Always check absence of capacitive coupling!
(rotation of coil by 180^0 should give identical signal but of opposite polarity)

Magnetic field

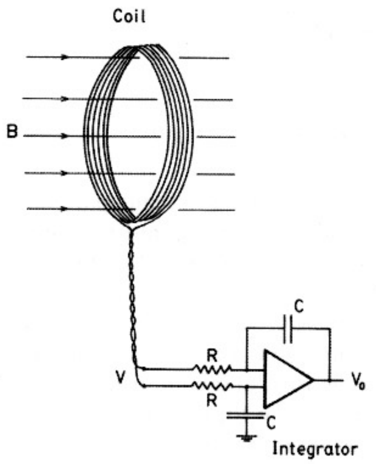

Magnetic coil

$$\oint_C \vec{E}\cdot d\vec{l} = -\iint_S \dot{\vec{B}}\cdot d\vec{s} \qquad V = NA\dot{B}$$

after integrator:

$$\boxed{B(t) = \frac{RC}{NA}\cdot V_{\text{int}}(t)}$$

Example of magnetic probe designed to measure magnetic field distribution inside the plasma

More often a set of coils outside

Always check absence of capacitive coupling!
(rotation of coil by 180^0 should give identical signal but of opposite polarity)

<u>Recent design</u>:
dif. ampl. of oppositely wounded coils ➔ (B_x, B_y, B_z) (100MHz)
[Everson et.al, RSI 80, 113505 (2009)]

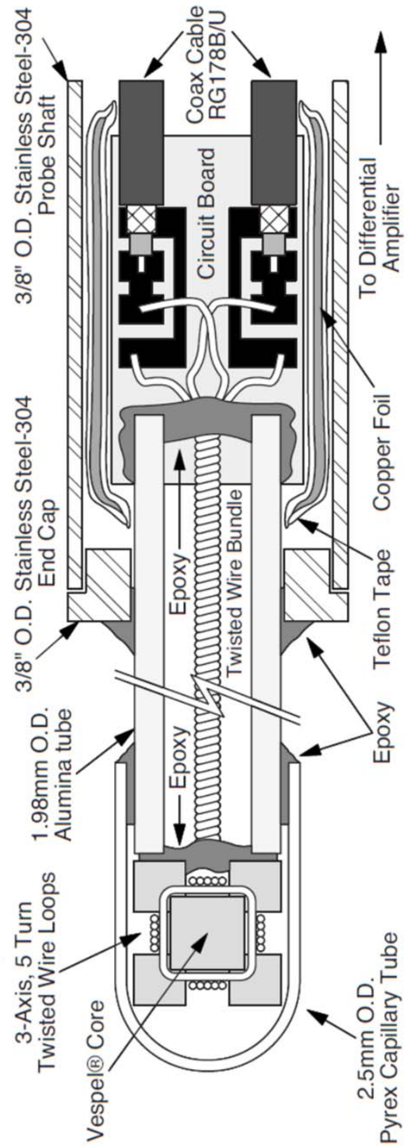

Magnetic field

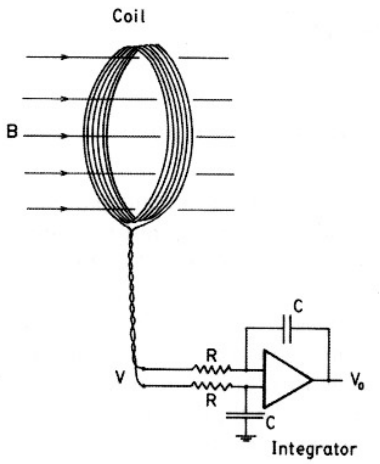

Magnetic coil

$$\oint_C \vec{E} \cdot d\vec{l} = -\iint_S \dot{\vec{B}} \cdot d\vec{s} \qquad V = NA\dot{B}$$

after integrator: $$\boxed{B(t) = \frac{RC}{NA} \cdot V_{\mathrm{int}}(t)}$$

Magnetic probes in HEDP:

- **Usually positioned at some distance from the object – require extrapolation of the measured signal to the object (sometimes by many orders of magnitude)**
- **Can be strongly affected by a "noise" from energetic particles generated in the system (can be tested using two oppositely-wound probes)**

B-probe

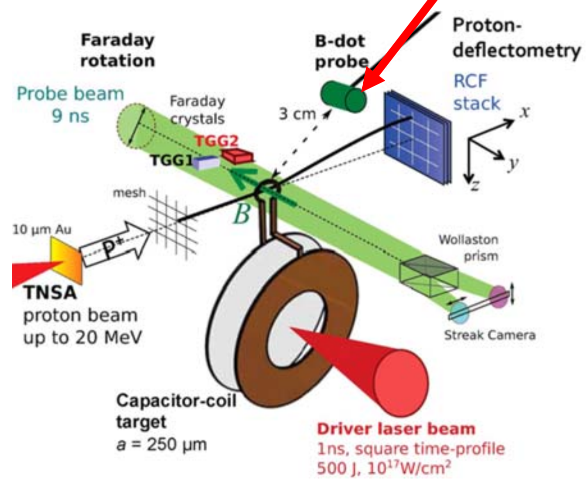

Measured: 5 mT at 3cm from the coil
Extrapolated: 800 T in the coil
➔ $800/5\times10^{-3} = 1.6\times10^{5}$

Santos *et al*, NJP, 17, 6083051 (2015)

Rogowski coil

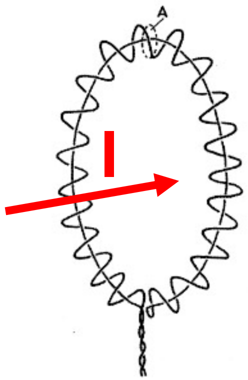

Gives total current through the loop, independent on current distribution.

(if the signal is not "too fast", i.e. τ > propagation time along the coil)

$$\Phi = n\oint_l \int_A dAB \cdot dl \qquad \oint_l B \cdot dl = \mu_0 I$$

$$\Phi = nA\mu_0 I \qquad \boxed{V = \dot{\Phi} = nA\mu_0 \dot{I}}$$

- **n is number of turns per unit length, A is area of the coil cross-section**
- **Induced voltage is proportional to dI/dt (V can be integrated before recording)**
- **"Return wire" to exclude contribution from magnetic flux through the coil**
- **needs electrostatic shielding**

s.lebedev@ic.ac.uk May 2019

Probing by E/M waves

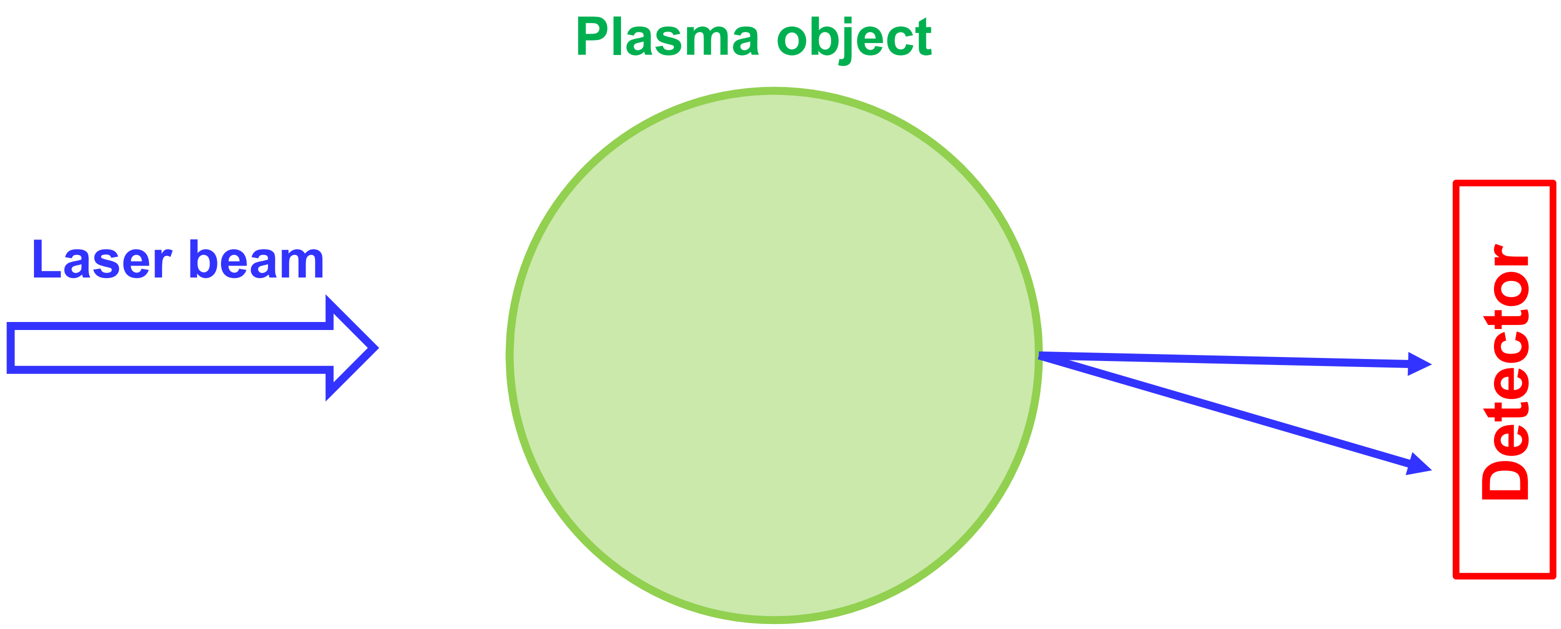

Change of phase velocity

Refraction of the beam (deflection, broadening)

Rotation of polarisation plane (Faraday effect)

Refractive index measurements

Propagation of electro-magnetic waves

$$V_{ph} = \frac{\omega}{k} = \frac{c}{\eta}$$

$\eta \neq 1 \;\Rightarrow$ **phase shift (interferometry)**

$\nabla\eta \neq 0 \;\Rightarrow$ **refraction of the beam (schlieren and sadowgraphy)**

$\eta_+ \neq \eta_- \Rightarrow$ **rotation of polarisation plane (Faraday effect)**

Refractive index of plasma without magnetic field:

$$\omega^2 = \omega_p^2 + k^2c^2 \quad \Rightarrow \quad \eta = \sqrt{(1 - \frac{\omega_p^2}{\omega^2})} = \sqrt{(1 - \frac{n_e}{n_{cr}})} \qquad n_{cr}\,[cm^{-3}] = \frac{1.12 \cdot 10^{21}}{\lambda^2\,[\mu m]}$$

Probing beam cannot propagate if the plasma density is above the critical density $\Longrightarrow$

Cut-off densities:

$\lambda = 337\mu m$ **(HCN laser)** $n_{cr} = 10^{16} cm^{-3}$

$\lambda = 10.6\mu m$ **(CO_2 laser)** $n_{cr} = 10^{19} cm^{-3}$

$\lambda = 1.06\mu m$ **(Nd, ω_0)** $n_{cr} = 10^{21} cm^{-3}$

$\lambda = 0.532\mu m$ **(Nd $2\omega_0$)** $n_{cr} = 4 \cdot 10^{21} cm^{-3}$

Interferometry

Mach-Zehnder and Michelson configurations

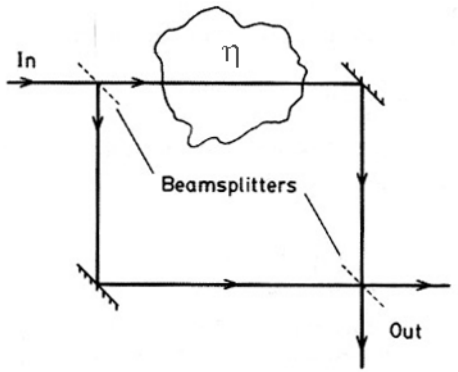

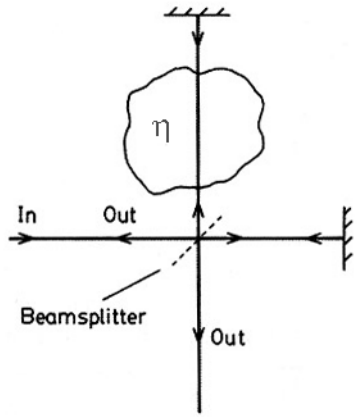

Signal on the detector:

$$E_t^2 = (E_r^2 + E_p^2)\cdot[1 + \frac{2E_rE_p}{(E_r^2 + E_p^2)}\cdot\cos(\varphi)]$$

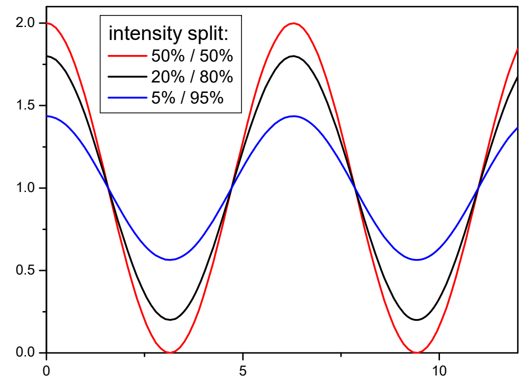

Equal intensities of the probing and reference beams give the best visibility of the fringes

Phase shift (typically $n_e \ll n_{cr}$):

$$\varphi = \int (k_p dl - k_r dl)$$

$$\varphi = \frac{\omega}{c}\int[\sqrt{1-\frac{n_e}{n_{cr}}} - 1]dl \approx -\frac{\omega}{2cn_{cr}}\int n_e dl$$

Number of fringes:

$$F = \frac{\varphi}{2\pi} = 4.46\cdot 10^{-18}\lambda_{[\mu m]}\cdot\int_{[cm^{-2}]} n_e dl$$

Line density corresponding to one fringe:

$\lambda = 337\mu m$ **(HCN laser)** $\langle n_e L\rangle = 6.6\cdot 10^{14} cm^{-2}$

$\lambda = 10.6\mu m$ **(CO_2 laser)** $\langle n_e L\rangle = 2.1\cdot 10^{16} cm^{-2}$

$\lambda = 1.06\mu m$ **(Nd, ω_0)** $\langle n_e L\rangle = 2.1\cdot 10^{17} cm^{-2}$

$\lambda = 0.532\mu m$ **(Nd $2\omega_0$)** $\langle n_e L\rangle = 4.2\cdot 10^{17} cm^{-2}$

For "cw" plasmas need to exclude vibrations (two wavelength interferometry)

Interferometry

Refractive index for neutral gases

$$\eta_a = 1 + (2\pi e^2 / m) \cdot \sum_{i,k} \frac{f_{i,k} n_i}{(\omega_{ik}^2 - \omega^2)}$$

$f_{i,k}$ is an oscillator strength for i to k transition

ω_{ik} is the frequency of transition

n_i is the density of atoms in state i

For optical frequencies far from spectral lines (α is polarizibility):

$$\eta_a \approx 1 + 2\pi\alpha \cdot n_a$$

Atom	$2\pi\alpha$
He	$1.3 \cdot 10^{-24}$ cm^3
H_2	$5 \cdot 10^{-24}$ cm^3
Air	$1.1 \cdot 10^{-23}$ cm^3
Ar	$1 \cdot 10^{-23}$ cm^3
Al	$4.4 \cdot 10^{-23}$ cm^3

Phase shift:

$$\varphi = \frac{2\pi}{\lambda} \int (1 - \eta) dl$$

Number of fringes due to electrons and atoms:

$$F = \frac{\varphi}{2\pi} = -4.46 \cdot 10^{-14} \cdot \lambda_{[cm]} \cdot \int n_e dl + \frac{2\pi\alpha}{\lambda} \cdot \int n_a dl$$

- different sign of phase shift for electrons and atoms

 [e.g. for H_2 φ=0 at n_e/n_a=2.2% (0.56% for He) @ 6943Å]

- different dependence on λ

s.lebedev@ic.ac.uk May 2019

Interferometry

Mach-Zehnder and Michelson configurations

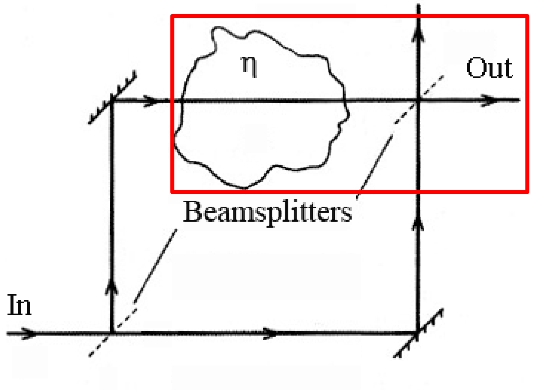

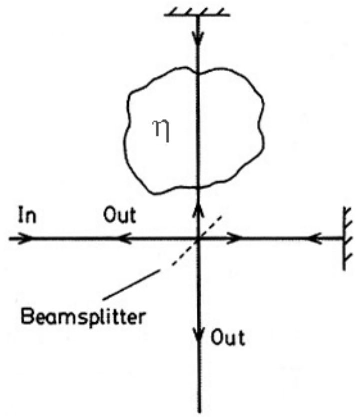

Signal on the detector:

$$E_t^2 = (E_r^2 + E_p^2)\cdot[1 + \frac{2E_rE_p}{(E_r^2 + E_p^2)}\cdot\cos(\varphi)]$$

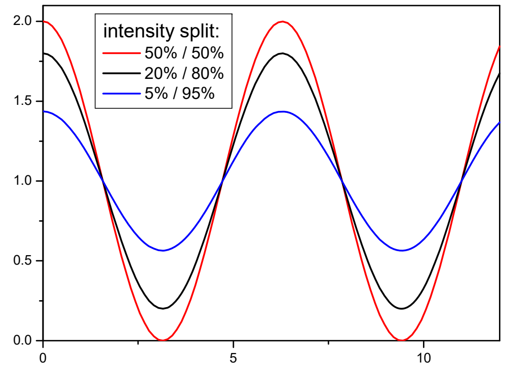

Equal intensities of the probing and reference beams give the best visibility of the fringes

Phase shift (typically $n_e << n_{cr}$):

$$\varphi = \int (k_p dl - k_r dl)$$

$$\varphi = \frac{\omega}{c}\int[\sqrt{1 - \frac{n_e}{n_{cr}}} - 1]dl \approx -\frac{\omega}{2cn_{cr}}\int n_e dl$$

Number of fringes:

$$F = \frac{\varphi}{2\pi} = 4.46\cdot 10^{-18}\lambda_{[\mu m]}\cdot\int_{[cm^{-2}]} n_e dl$$

Line density corresponding to one fringe:

$\lambda = 337\mu m$ (HCN laser) $\langle n_e L\rangle = 6.6\cdot 10^{14} cm^{-2}$

$\lambda = 10.6\mu m$ (CO_2 laser) $\langle n_e L\rangle = 2.1\cdot 10^{16} cm^{-2}$

$\lambda = 1.06\mu m$ (Nd, ω_0) $\langle n_e L\rangle = 2.1\cdot 10^{17} cm^{-2}$

$\lambda = 0.532\mu m$ (Nd $2\omega_0$) $\langle n_e L\rangle = 4.2\cdot 10^{17} cm^{-2}$

For “cw” plasmas need to exclude vibrations (two wavelength interferometry)

Interferometric imaging

Wide probing and reference beams to produce 2-D image of plasma

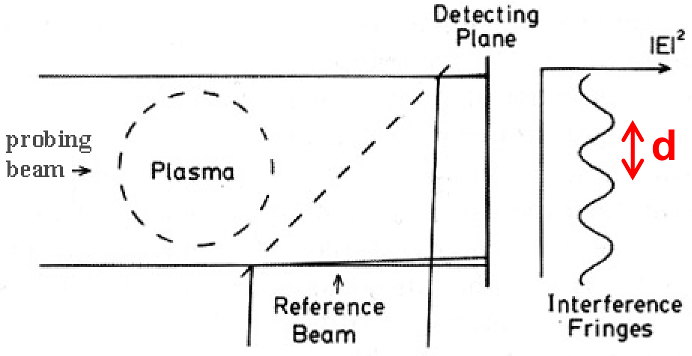

Misalignment between the beams (α)

$\Downarrow$

reference fringes ($d = \lambda / [2 \cdot \sin(\alpha/2)]$) in the regions without plasma

Fringe shift due to plasma $\Rightarrow$ map of $\langle n_e L \rangle$

Practical lower limit ~1/10 – 1/30 of fringe

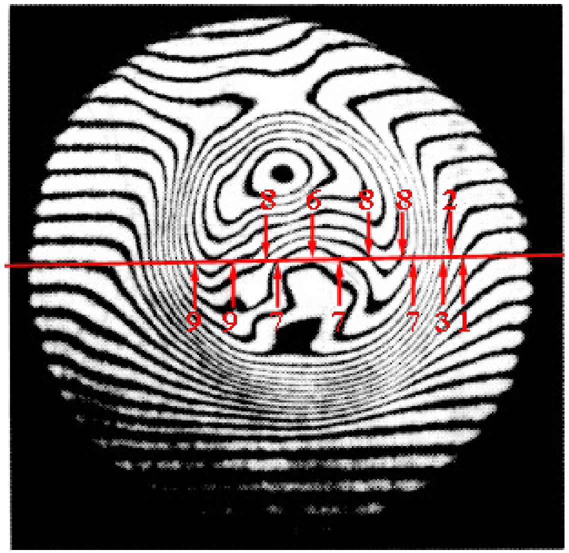

Numbers show fringe-shift in a particular position

Shear interferometer (best for small plasma objects)

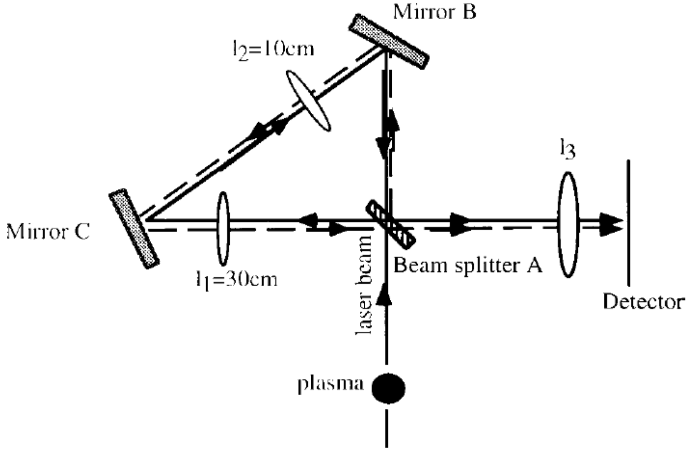

Magnified beam is used as a reference

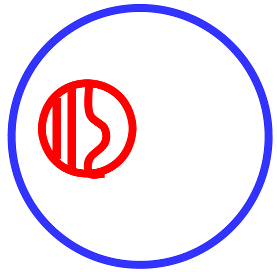

M. Tatarakis *et al*, PoP, 5, 682 (1998)

Simple Example: Interferogram of 8 Wire Tungsten Array

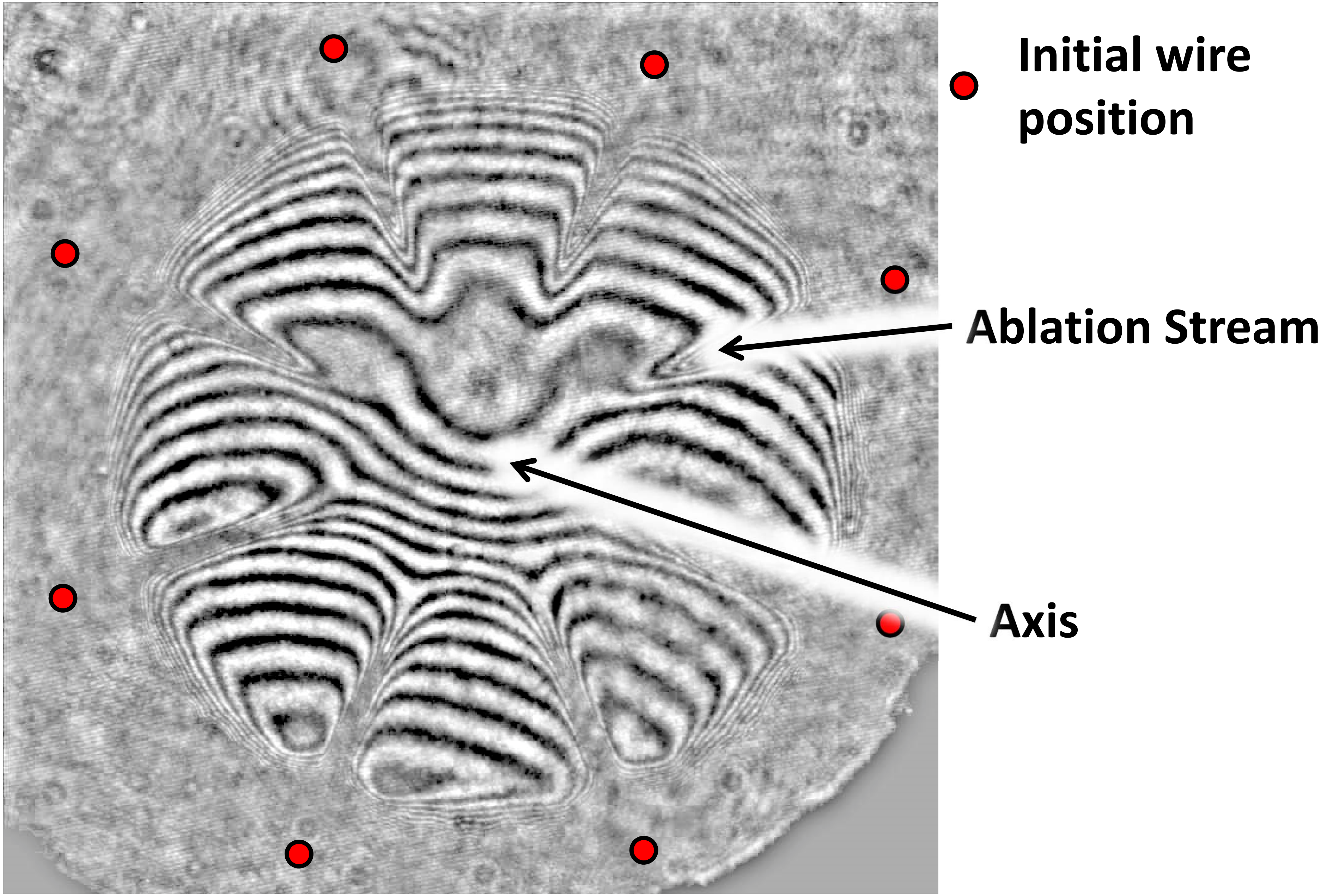

Analysis method: [Swadling et al. - PoP **20**, 022705 (2013)]

Trace <u>experimental</u> and <u>background</u> fringes:

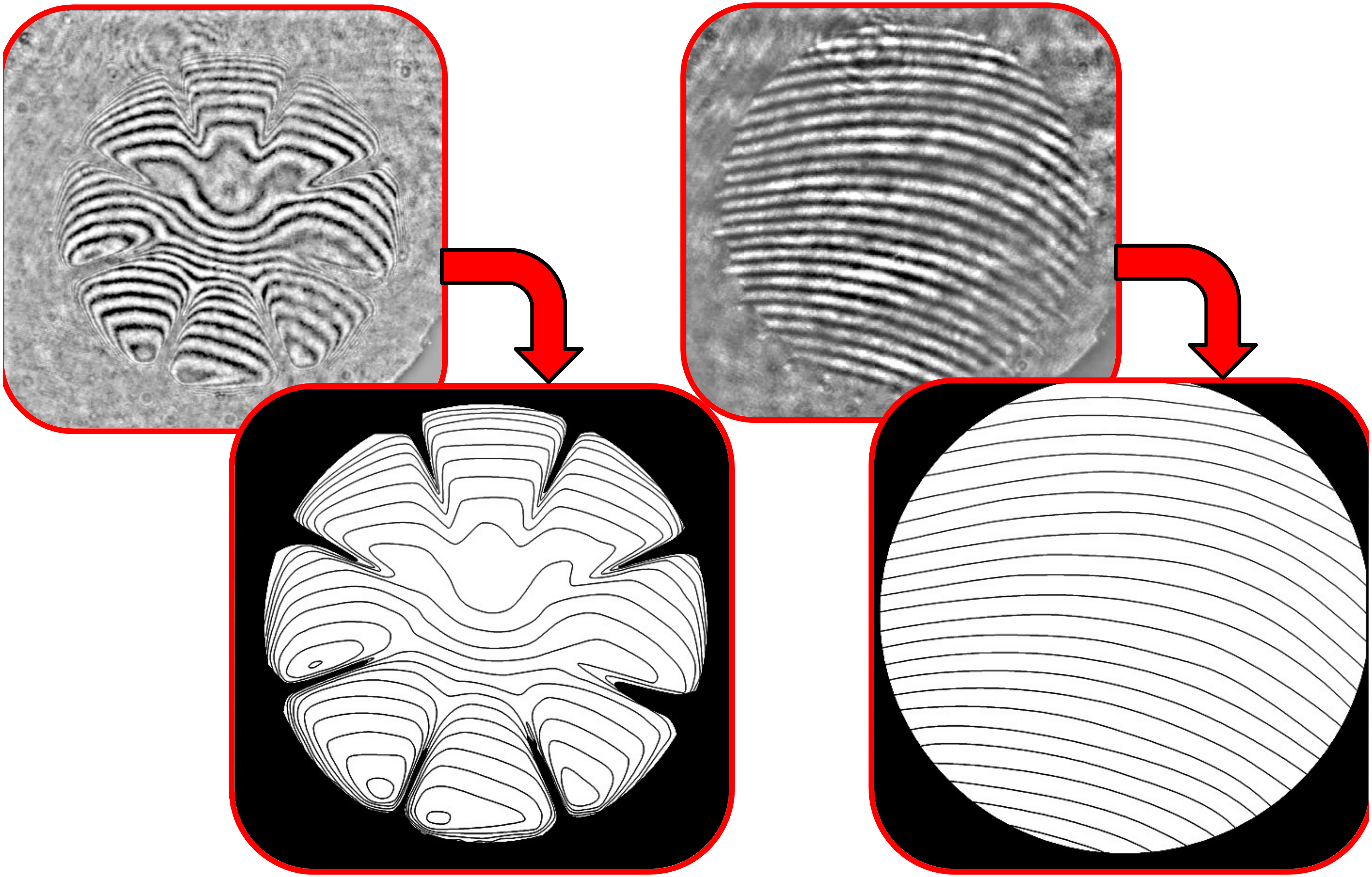

Number fringes, interpolate and subtract

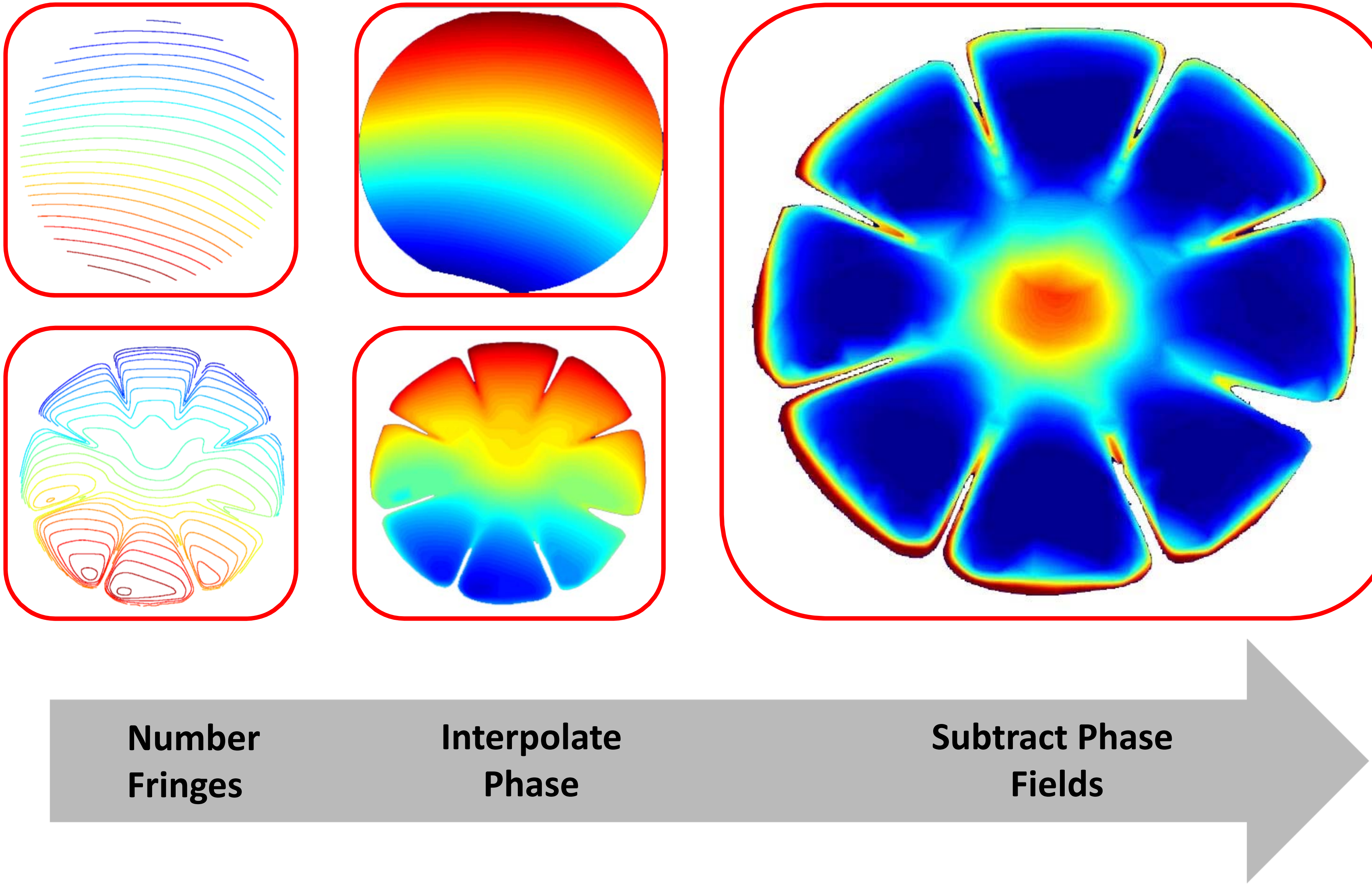

More Complex example – 32 wire Al array

Results published - ***Swadling et al. -*** Physics of Plasmas **20**, 022705 (2013).

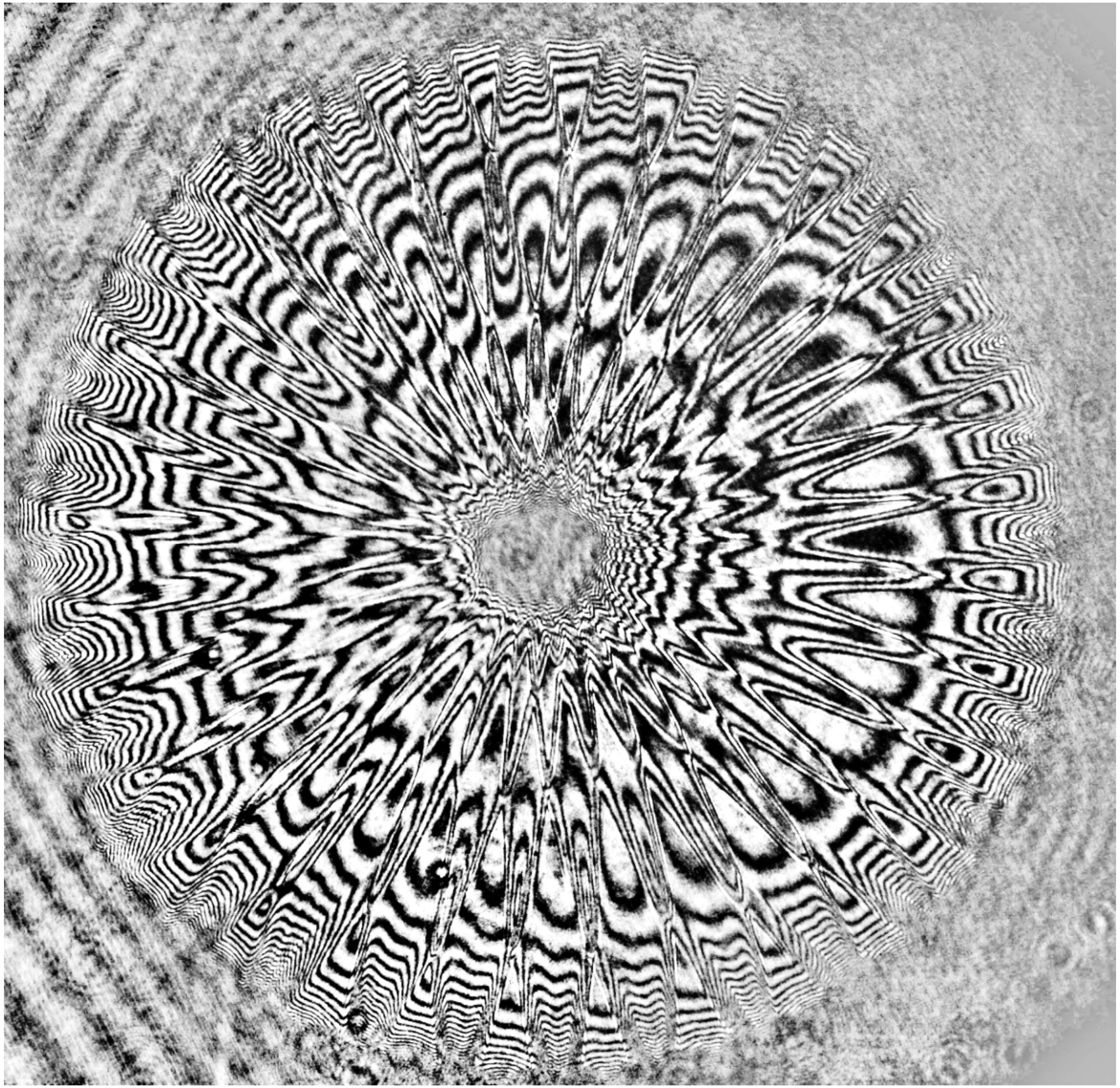

More Complex example – 32 wire Al array

Results published - ***Swadling et al. -*** Physics of Plasmas **20**, 022705 (2013).

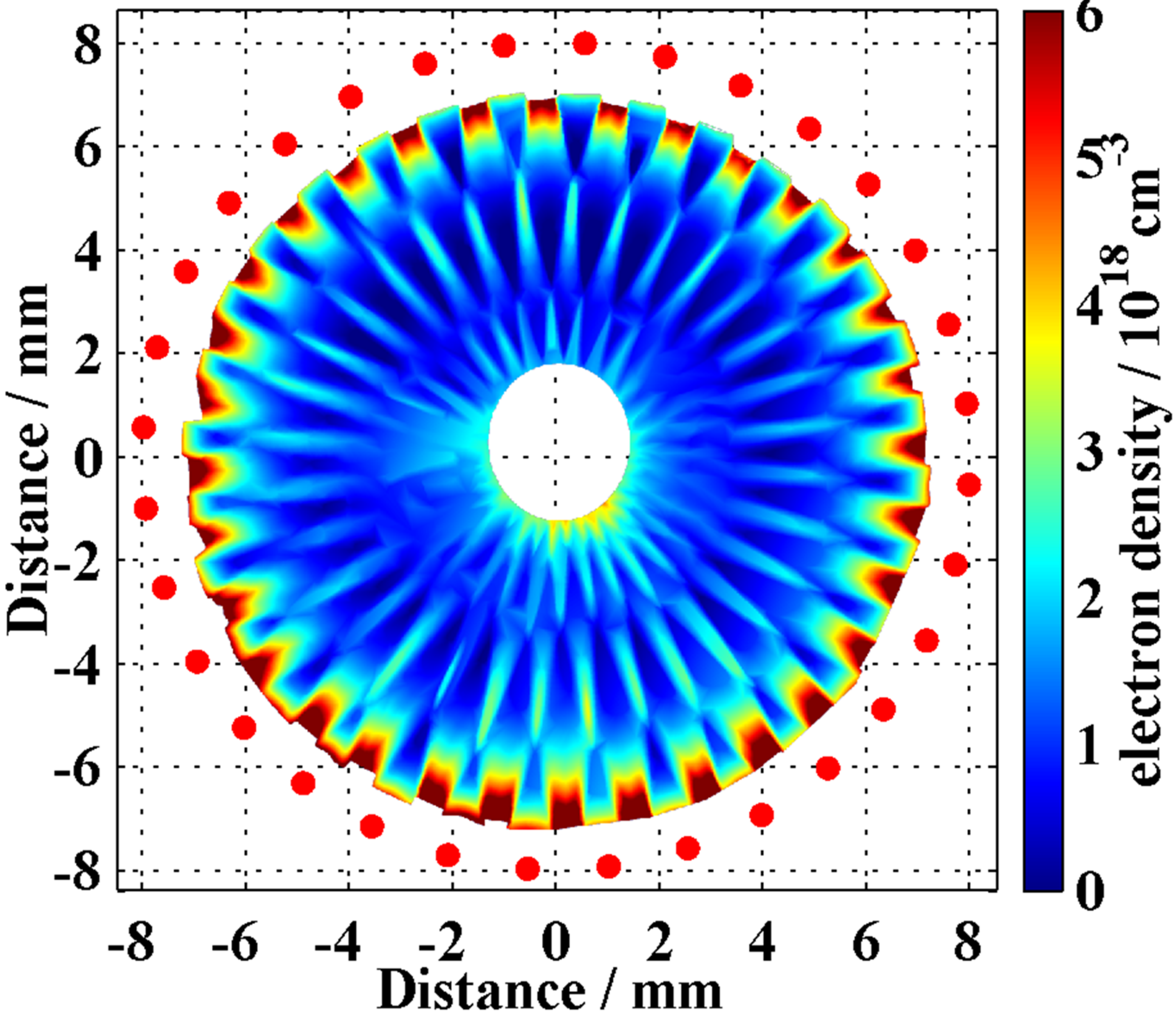

Schlieren and shadow imaging

Transverse density gradients deflect the probing beam

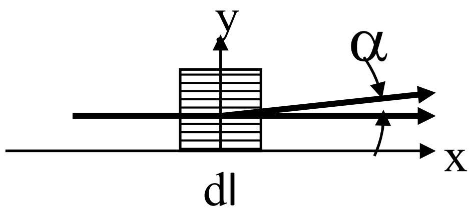

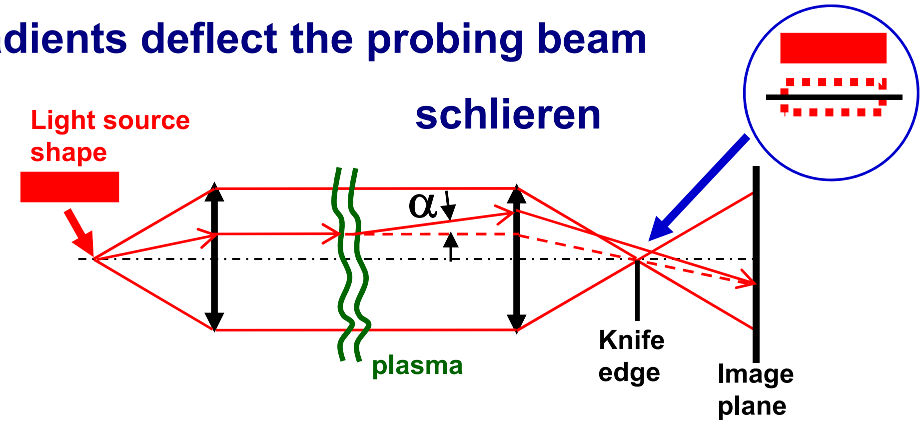

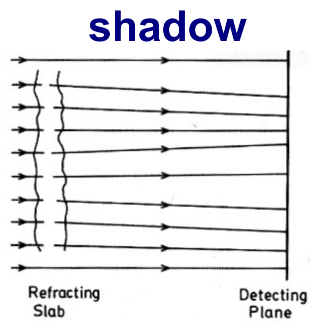

Deflection angle:

$$\alpha = \frac{d}{dy}\int \eta dl \approx \frac{1}{2n_{cr}}\frac{d}{dy}\int n_e dl$$

Example:

$\alpha = 2 \cdot 10^{-3}$rad, $\lambda = 532$nm

$\int \nabla n_e dl = 1.5 \cdot 10^{19}$cm^{-3}

Knife to measure 1-D gradients

pin-hole for “bright-field” schlieren

disk for “dark-field” schlieren

Bow-shock at an obstacle

Jet boundary shock

Supersonic plasma jet

Intensity distribution

$$\frac{\Delta I}{I} = L\left[\frac{d^2}{dx^2} + \frac{d^2}{dy^2}\right]\int \eta dl$$

(If an imaging system between the object and the detection plane is used, then *L* is the plasma length)

s.lebedev@ic.ac.uk May 2019

Example: plasma jet – obstacle interaction

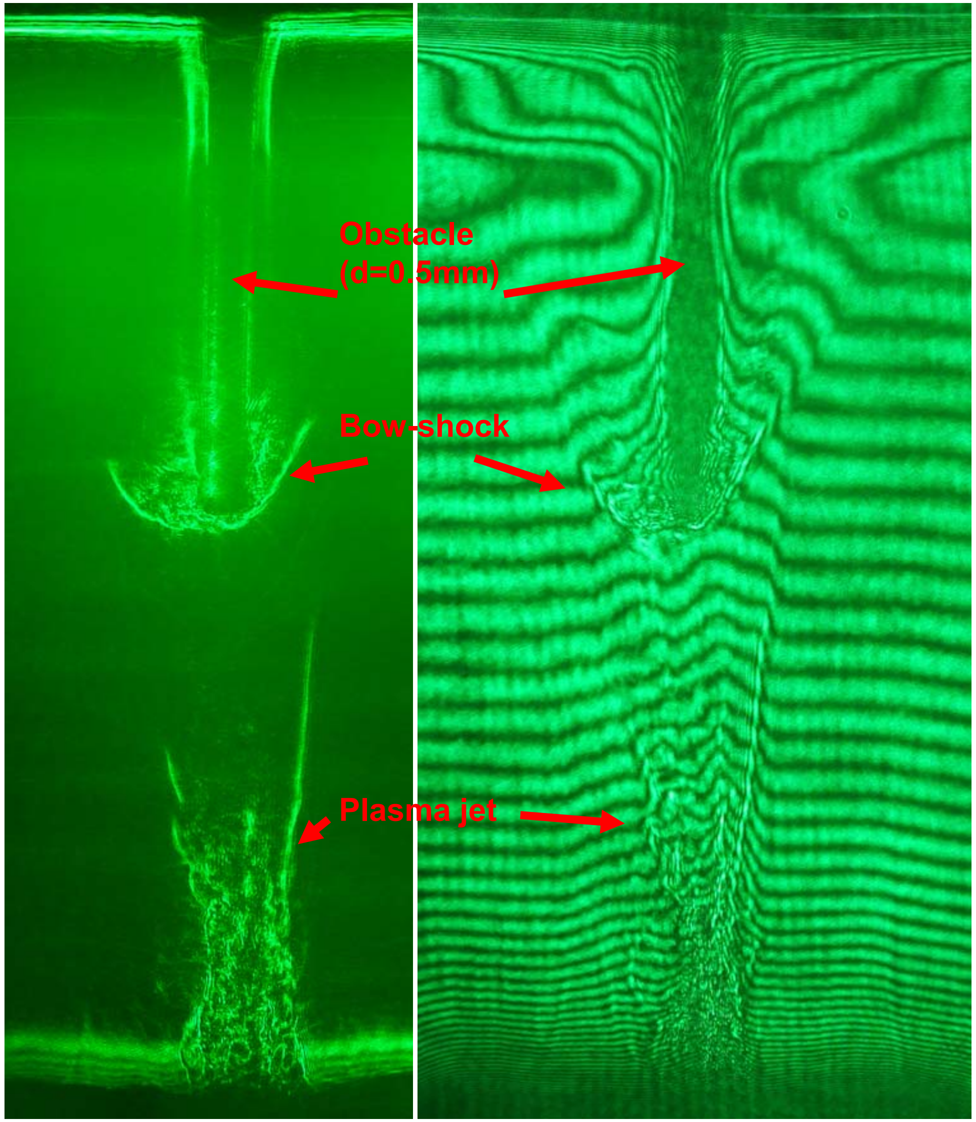

Flow direction

Supersonic magnetized plasma jet interacts with an obstacle (experiments on MAGPIE facility at Imperial College):

$n_e \sim 10^{18}\mathrm{cm}^{-3}$, $V_{jet} \sim 100\mathrm{km/s}$,

$\alpha = 5 \cdot 10^{-3}\mathrm{rad}$, $\lambda=532\mathrm{nm}$

Schlieren image highlights the positions of sharp gradients: bow-shock and collimation shock at the jet boundary

Interferogram allows measurements of the electron density in the regions where interference fringes are traceable

Faraday rotation

Linearly polarised wave is superposition of two circularly polarised.

Difference in refractive indexes of the two waves leads to rotation of polarisation plane

Rotation of polarisation plane:

$$\alpha = \frac{e}{2m_e c}\int \frac{n_e \vec{B}\cdot d\vec{l}}{n_{cr}(1-n_e/n_{cr})^{1/2}} \approx \frac{e}{2m_e c}\int \frac{n_e}{n_{cr}}\vec{B}\cdot d\vec{l}$$

$$\alpha_{[rad]} = 2.26\cdot 10^{-17}\lambda^2_{[cm]}\int n_{e[cm^{-3}]}\vec{B}_{[G]}\cdot d\vec{l}$$

Example:

$n_e=10^{19}$ cm^{-3}, B=10^5G (10T), λ=532nm, *L*=1cm => α =3.67^0

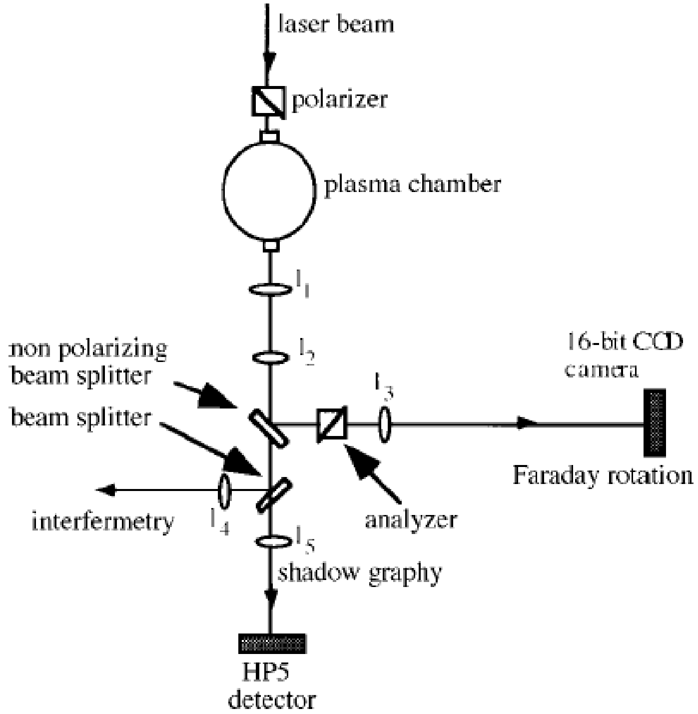

Magnetic field can be found if the density distribution is known

Convenient to combine with interferometry

M. Tatarakis *et al*, PoP, 5, 682 (1998)

Faraday rotation

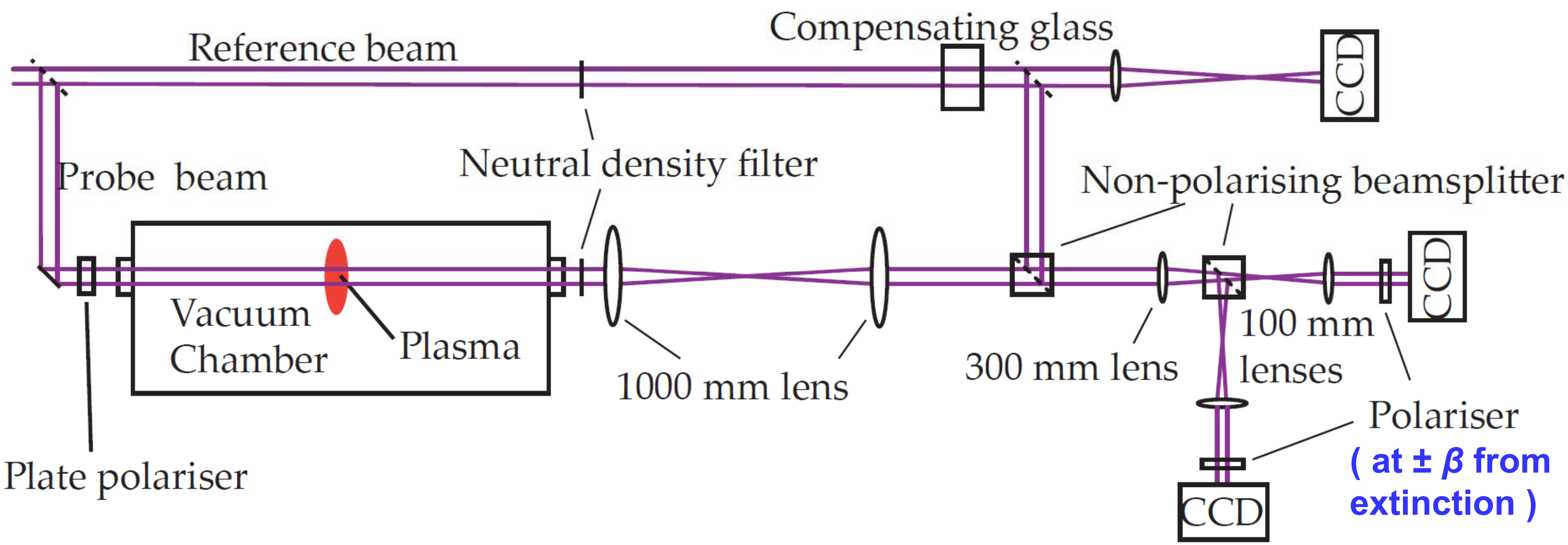

Detector sensitivity; Probe beam intensity; Faraday rotation angle; Polariser angle; Self-emission

$$I_{S\pm} = s_{\pm}(x,y)\cdot\left[I_S(x,y)\cdot \sin^2(\alpha(x,y)\pm\beta)+\frac{I_{SE}(x,y)}{2}\right]$$

$$I_{B\pm} = s_{\pm}\cdot I_B\cdot \sin^2(\beta)$$

$$\alpha(x,y)=\frac{1}{2}\cdot \sin^{-1}\left[\frac{I_B(x,y)}{I_S(x,y)}\left\{\frac{I_{S+}(x,y)}{I_{B+}(x,y)}-\frac{I_{S-}(x,y)}{I_{B-}(x,y)}\right\}\cdot\frac{\tan(\beta)}{2}\right]$$

G. Swadling *et al*, RSI, 85, 11E502 (2014)

Example of Faraday rotation measurements

Interaction with conducting obstacle

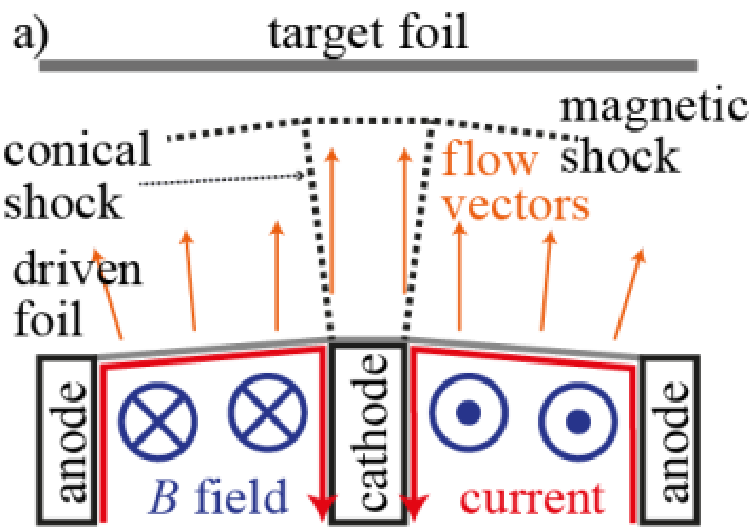

Polarimetry images: two channels

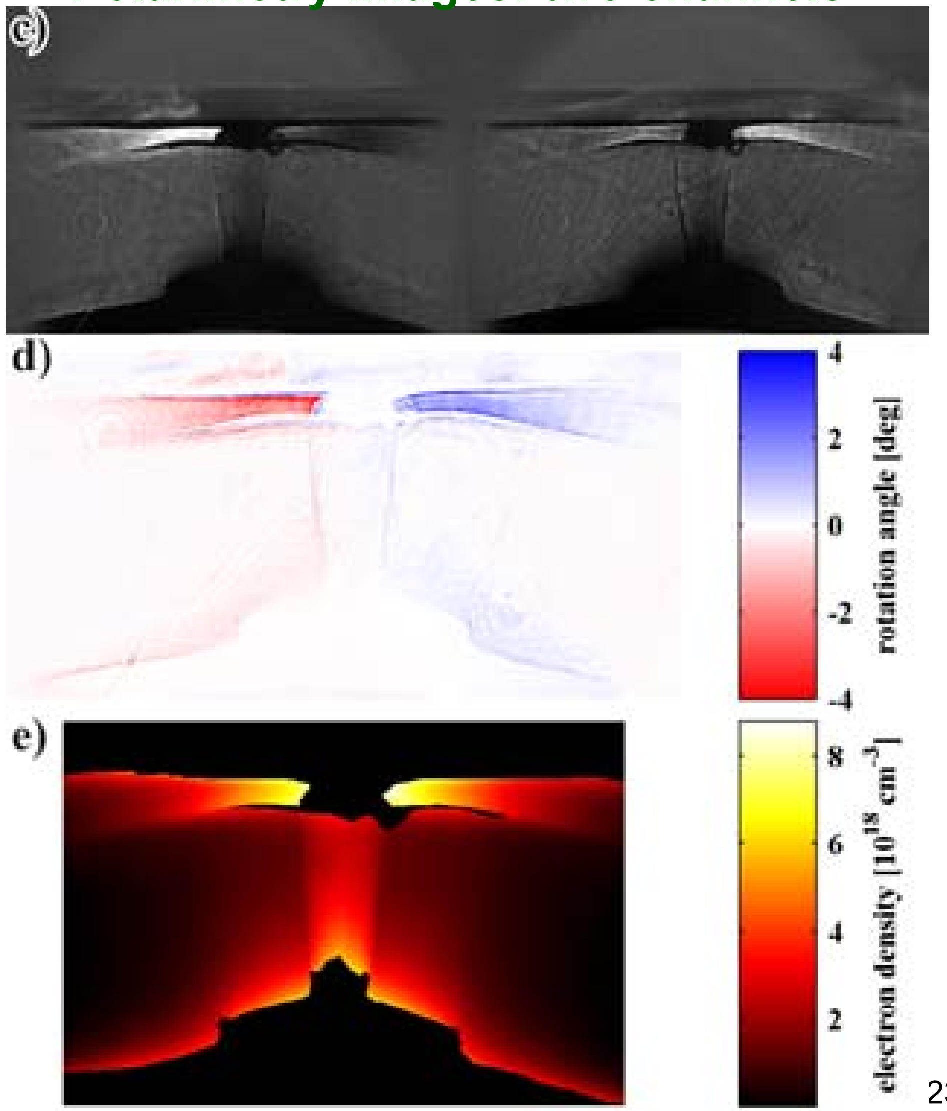

s.lebedev@ic.ac.uk May 2019

Abel inversion

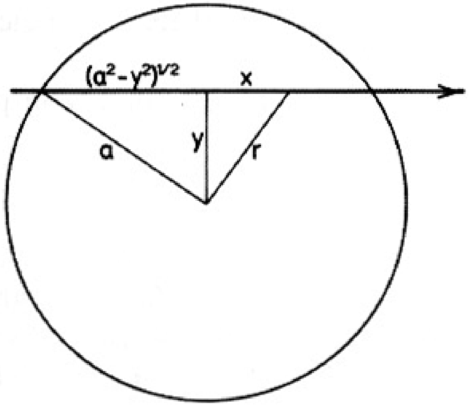

Many diagnostics measure a particular plasma parameter integrated along probing path.

For a cylindrically symmetric object it is possible to reconstruct radial distribution from several chord integrals

$$F(y) = \int f(r)dx = 2\int_y^a f(r)\frac{rdr}{\sqrt{(r^2-y^2)}}$$

Chord integral of e.g. phase shift, rotation angle or radiative emissivity

$$f(r) = -\frac{1}{\pi}\int_r^a \frac{dF}{dy}\frac{dy}{\sqrt{(y^2-r^2)}}$$

Radial profile of quantity F

Accuracy of reconstruction strongly depends on errors in dF/dy $\Rightarrow$ need to have sufficiently large number of chords and low level of "noise"

Outline

Electrical measurements: magnetic field and current

Laser probing: interferometry, density gradients

Emission: spectral lines, continuum

Thomson scattering

X-ray imaging

Proton probing

Continuum radiation

<u>Free-free</u> (bremsstrahlung)

$$j_{ff}(\nu) \sim n_e n_i Z_i^2 T^{-0.5} e^{-h\nu/kT_e}$$

<u>Free-bound</u> (recombination on level n)

$$j_{fb}(\nu) \sim n_e n_i Z_i^4 T^{-3/2} e^{(I_n - h\nu)/kT_e}$$

j(ν) is spectral power per unit frequency

divide by λ^2 if need $j(\lambda)$!

Temperature measurements from the slop of continuum radiation (hν > kT_e – typically from X-ray spectrum)

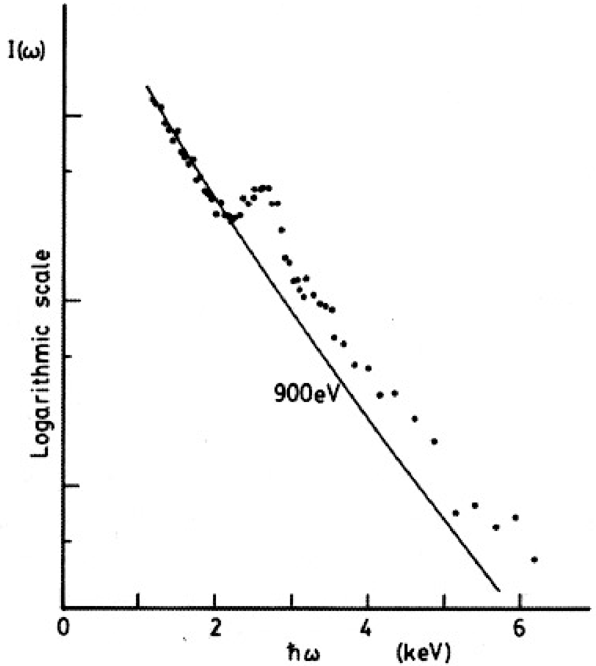

Density (Z_{eff}) measurements from absolute intensity (for hν << kT_e – in visible) if temperature is known

(weak dependence on temperature)

$$j(\lambda) \sim \frac{n_e^2 Z_{eff}}{T^{1/2}} \qquad \sum_i n_e n_i Z_i^2 \equiv n_e^2 Z_{eff}$$

need to chose spectral region free of lines

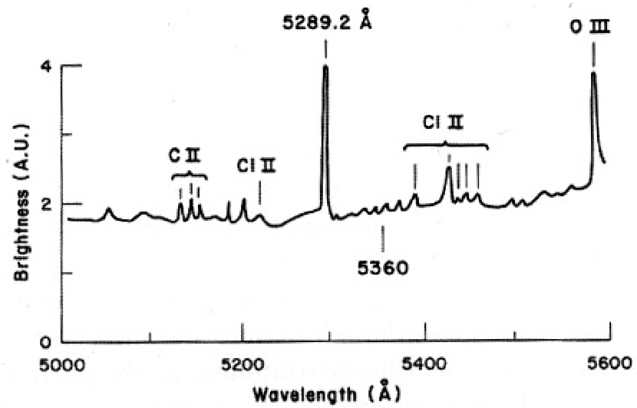

s.lebedev@ic.ac.uk May 2019

Continuum radiation

Black-body spectrum

$$j_{bb}(\nu) \sim \frac{h\nu^3}{e^{h\nu/kT} - 1}$$

$$j(\lambda) = \frac{1.19 \cdot 10^{20}}{\lambda_{\dot{A}}^5 \cdot \left(e^{\left(\frac{12395}{\lambda_A T_{eV}}\right)} - 1\right)} \; [W / cm^2 / \dot{A} / ster]$$

Transmission Grating Spectrometer

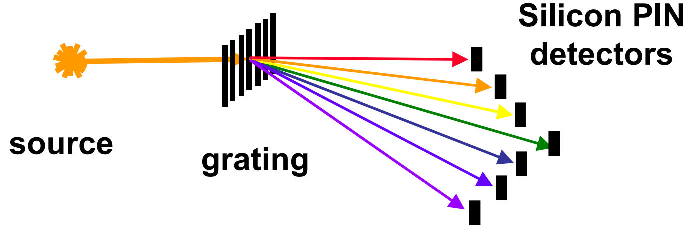

Differential filtering

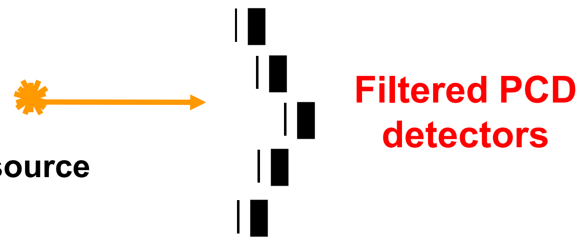

Radiation spectrum of tungsten Z-pinch

Cuneo et al, PoP 2001

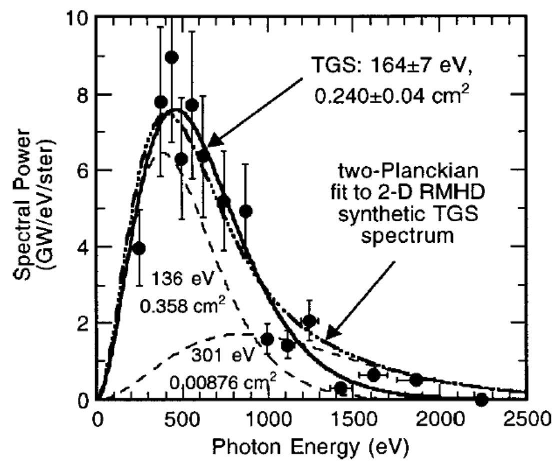

Hohlraum temperature on Z

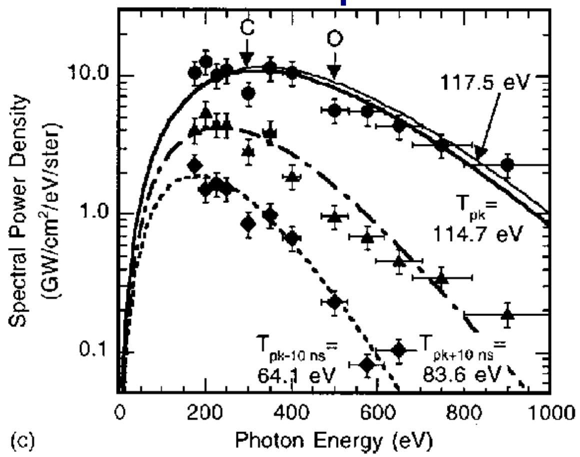

Relative intensities of spectral lines

$$j = \frac{h\nu_{ki}}{4\pi} A_{ki} n_k$$

$$A_{ki} = 6.67 \cdot 10^{15} \frac{g_i}{g_k} \frac{f_{ik}}{\lambda_{\dot{A}}^2}$$

A_{ki} is transition probability for spontaneous emission [s^{-1}]

n_k is number of atoms (ions) in the upper state [cm^{-3}]

f_{ik} is the "oscillator strength", usually used in spectroscopy

Need to know how population of different states depends on plasma parameters!

Local Thermodynamic Equilibrium (LTE).

$$\frac{n_k}{n_0} = \frac{g_k}{g_0} \exp\left(-\frac{E_k}{kT}\right)$$

Boltzmann distribution

$$\Downarrow$$

$$\frac{j_1}{j_2} = \frac{A_1}{A_2} \frac{g_1}{g_2} \exp\left(-\frac{\Delta E}{kT}\right)$$

Temperature from the ratio of line intensities

$$n_e[cm^{-3}] > 9 \cdot 10^{17} \left(\frac{T}{E_H}\right)^{1/2} \left(\frac{\Delta E}{E_H}\right)^3$$

$$(E_H = 13.6eV)$$

LTE is a good approximation at high density, when collisional transitions dominate over radiative

Griem, H.R., "Plasma spectroscopy"

Relative intensities of spectral lines

Coronal Equilibrium

$$\frac{dn_k}{dt} = n_e n_0 \langle \sigma_{1k} V \rangle - \sum_{j \neq k} n_k A_{kj} = 0$$

Collisional excitation balanced by radiative de-excitation

$$\frac{n_k}{n_0} = \frac{n_e \langle \sigma_{0k} V \rangle}{\sum_j A_{kj}} \propto f(T)$$

Population of levels depends on temperature

Collisional Radiative models (equilibrium or time-dependent)

Fractional abundances of Al ions

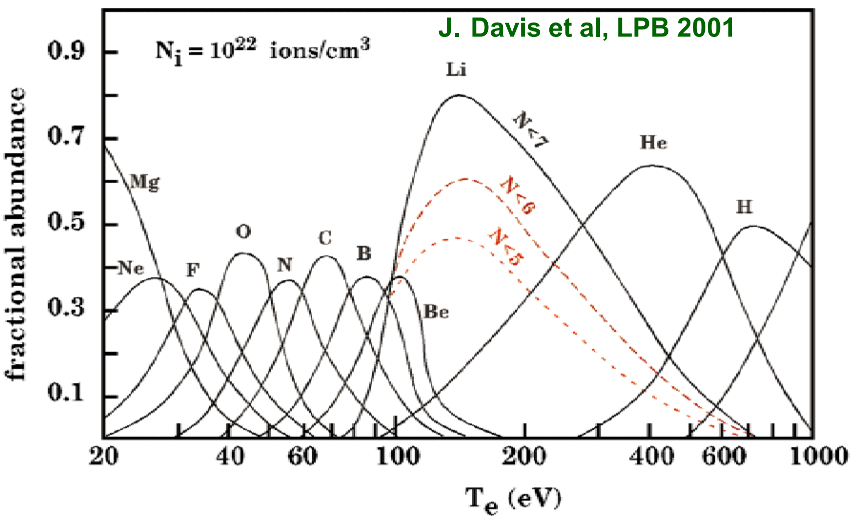

Line ratio (Al) as function of T_e and N_i

J.P. Apruzese et al, JQSRT 1997

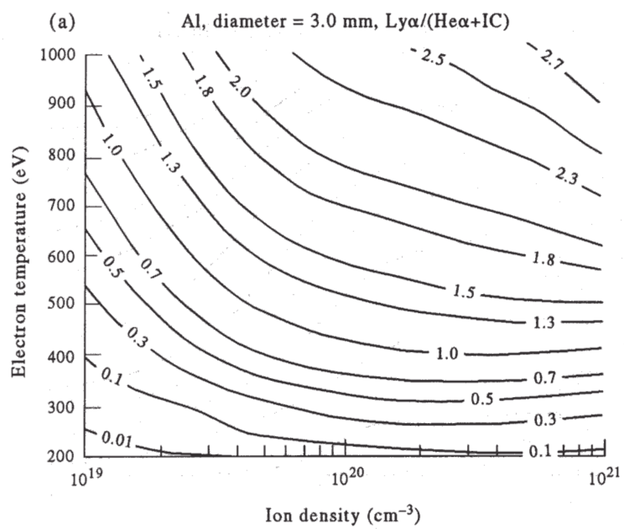

X-ray spectrum of a 600eV Al plasma

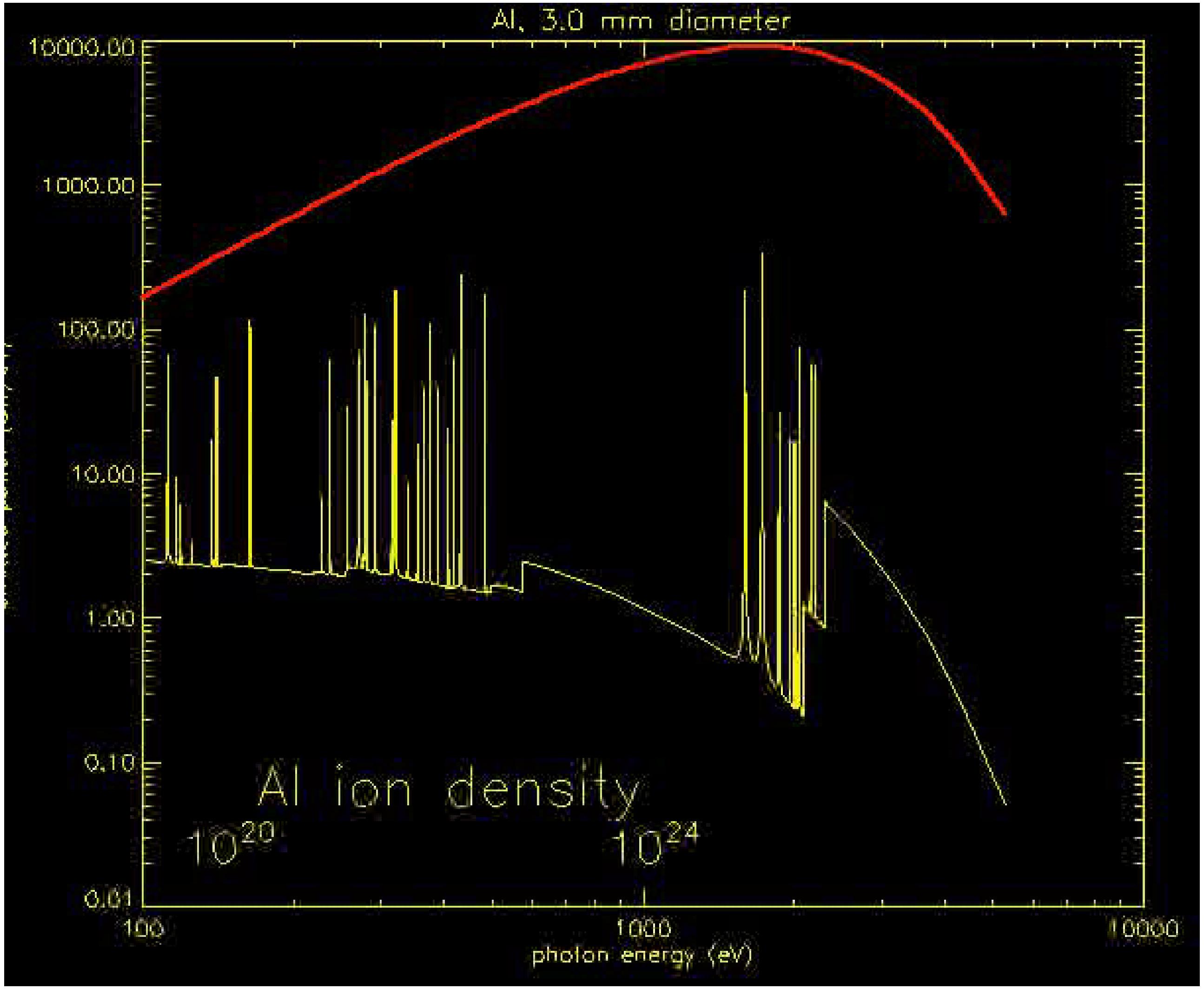

J. Apruzese, NRL (2001)

Effect of density on emission spectrum from 3mm diameter Al plasma

- **Lines and continuum**
- **Saturation at blackbody level**
- **Line "inversion" at high densities due to self-absorption**

X-ray spectrum of a 600eV Al plasma

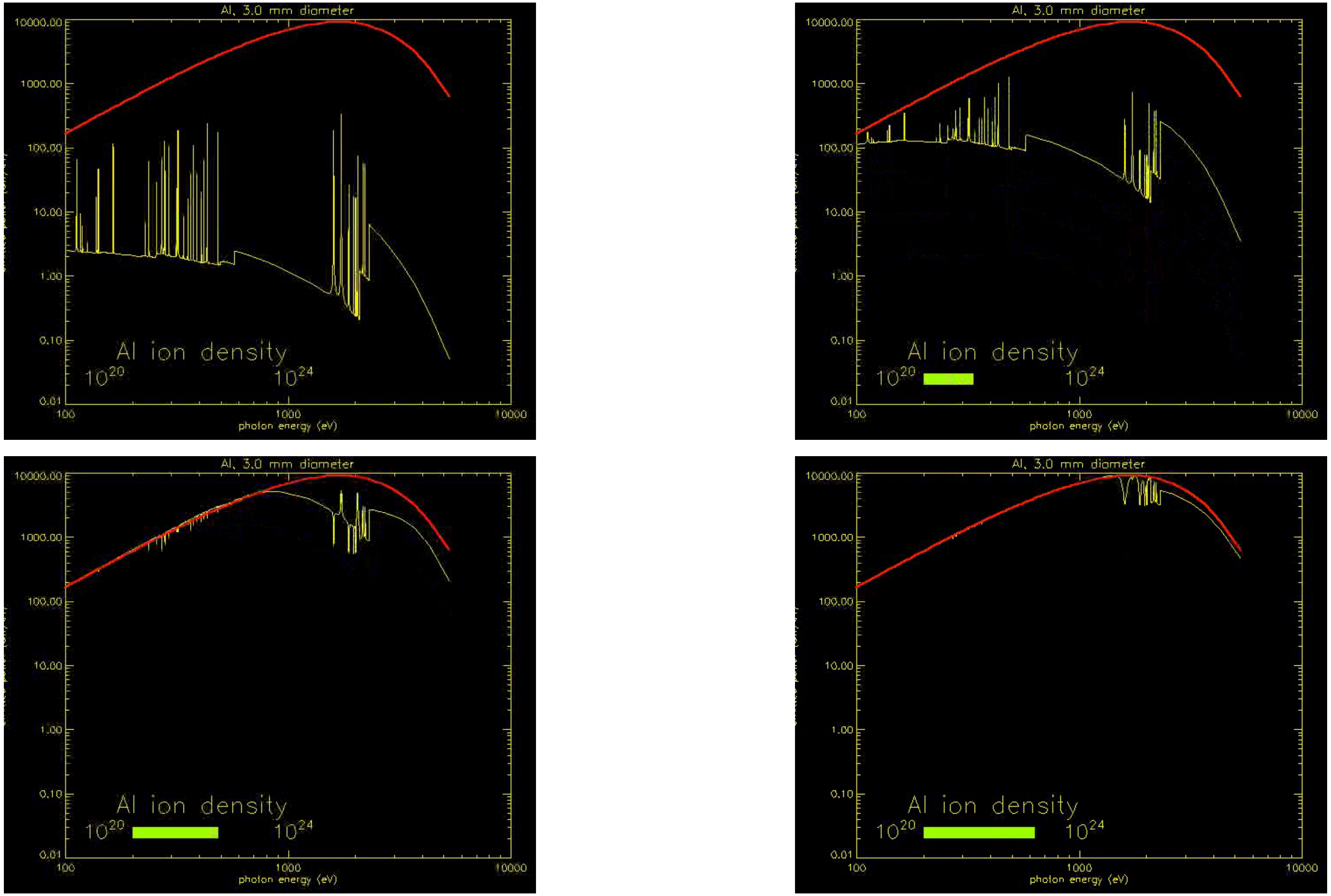

J. Apruzese, NRL (2001)

Spectral line broadening

Doppler broadening

Line profile for Maxwellian distribution:

$$I(\nu) = I(\nu_0)\exp\left(-\frac{(\nu-\nu_0)^2 c^2}{2V_T^2\nu_0^2}\right)$$

Ion temperature from $\Delta\lambda/\lambda$

$$T_i[eV] = 1.68\cdot 10^8 \frac{m_i}{m_H}\left(\frac{\Delta\lambda_{1/2}}{\lambda_0}\right)^2$$

Also for measurements of directed velocity

e.g. for H_β at T_i=100eV $\Delta\lambda$ ~ 3.7Å

Problem - choice of line (in X-rays $\Delta\lambda$ is too small)

Stark broadening (in electric field produced by neighbouring particles)

Characteristic E field:

$$E \propto \frac{e}{r^2} \sim n_i^{2/3}$$

Characteristic $\Delta\lambda$ (FWHM) (for H_β (λ=4861 Å)):

$$\Delta\lambda_{1/2}[\dot{A}] = 0.4\cdot\left(\frac{n[cm^{-3}]}{10^{14}}\right)^{2/3}$$

e.g. $\Delta\lambda$ ~ 1.8 Å for $n_i=10^{15}cm^{-3}$

Stark-broadened hydrogen lines (Balmer)

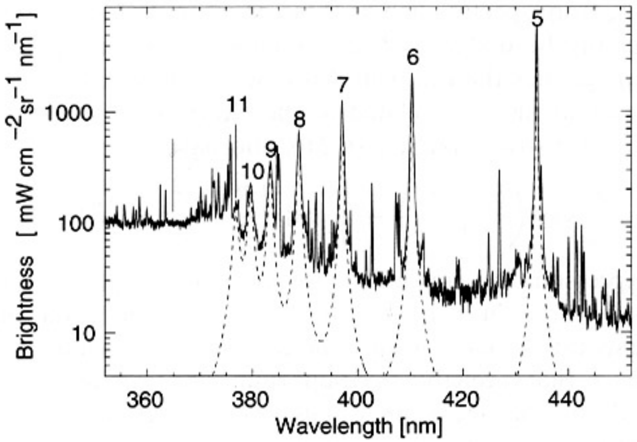

s.lebedev@ic.ac.uk May 2019

Zeeman splitting

$$\Delta\lambda_{[A]} = (M_2 g_2 - M_1 g_1)\lambda_{[A]}^2 \cdot 4.7 \cdot 10^{-13} B_{[G]}$$

Example: Li beam excited by dye laser

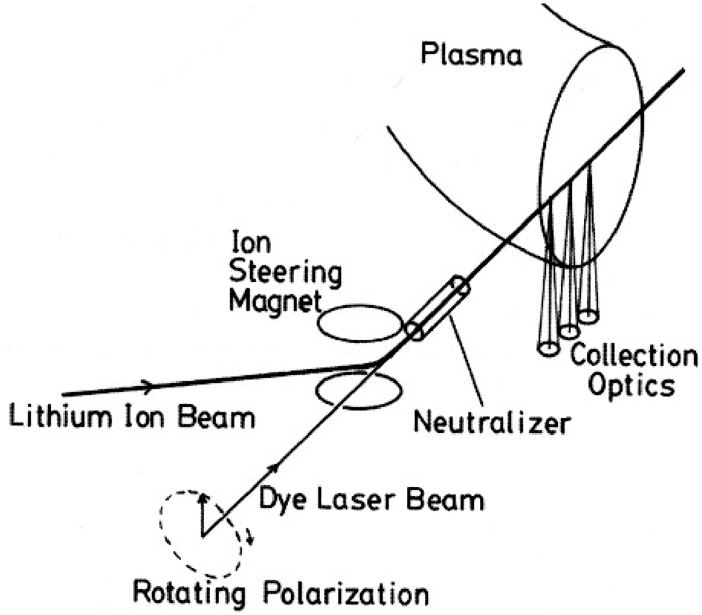

Usually difficult to find a suitable spectral line!

($\Delta\lambda/\lambda \sim \lambda$ – hard in X-rays)

Zeeman splitting

$$\Delta\lambda_{[A]} = (M_2 g_2 - M_1 g_1)\lambda_{[A]}^2 \cdot 4.7 \cdot 10^{-13} B_{[G]}$$

Example: laser plasma in magnetic field

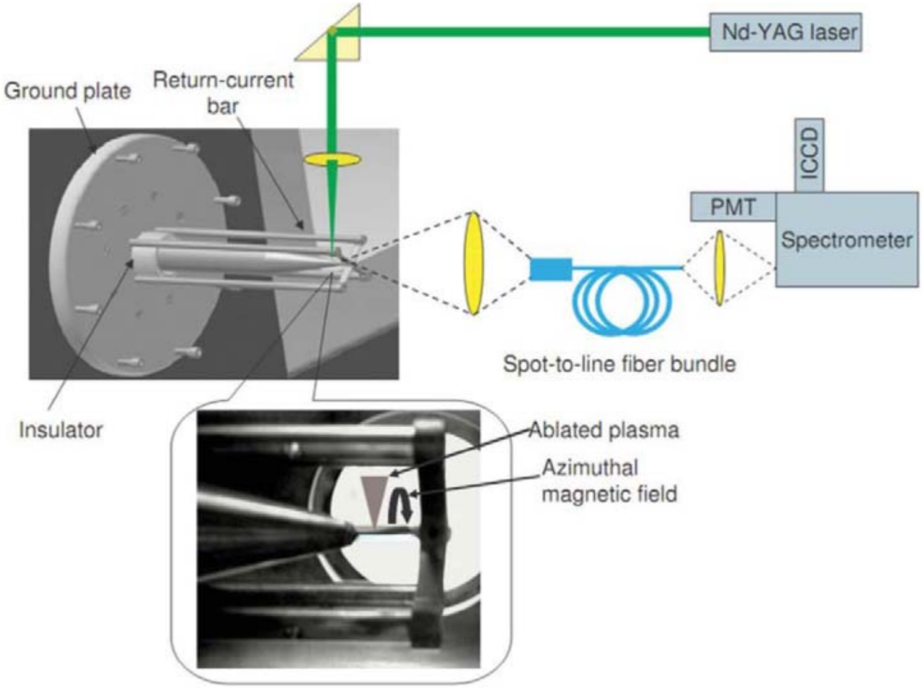

Al III 4s-4p ($^2S_{1/2} - {}^2P_{1/2}$ vs $^2S_{1/2} - {}^2P_{3/2}$)

Different sensitivity to B-field:

Zeeman splitting – B-field.

Stark broadening – n_e

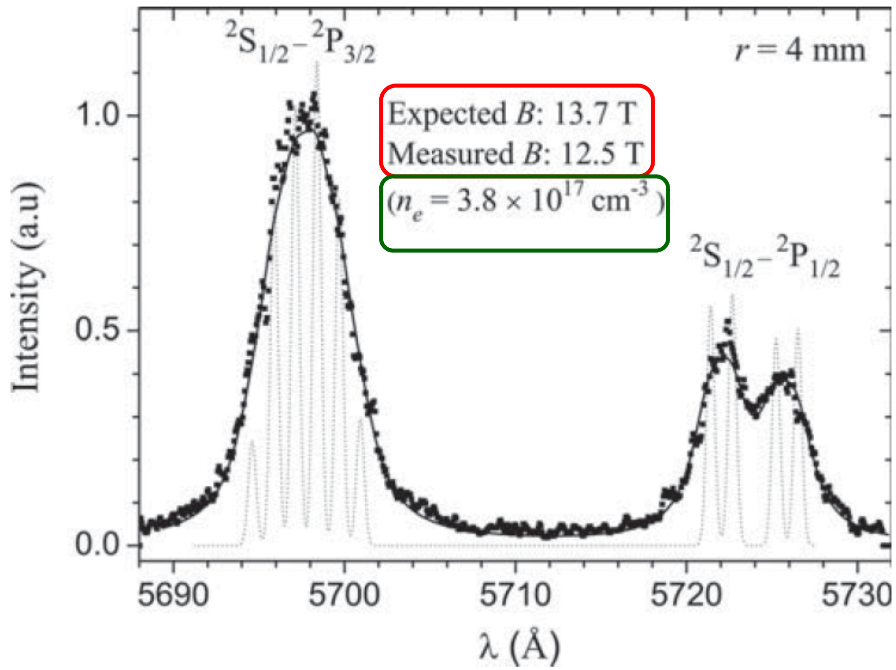

S. Tessaring *et al.*, PoP, 18, 093301 (2011)

Outline

Electrical measurements: magnetic field and current

Laser probing: interferometry, density gradients

Emission: spectral lines, continuum

Thomson scattering

X-ray imaging

Proton probing

s.lebedev@ic.ac.uk

Thomson scattering (optical)

Scattering of e/m radiation by <u>single electron</u>

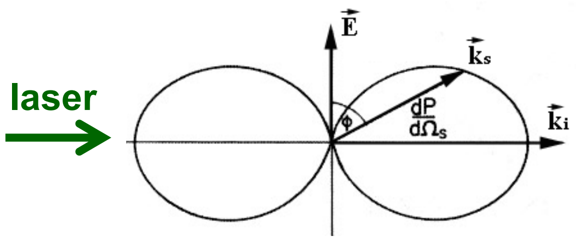

$$\frac{d\sigma}{d\Omega} = r_e^2 \sin^2(\phi)$$

$$\sigma = \frac{8\pi}{3} r_e^2 = 6.65 \cdot 10^{-25}\, cm^2$$

scattering geometry

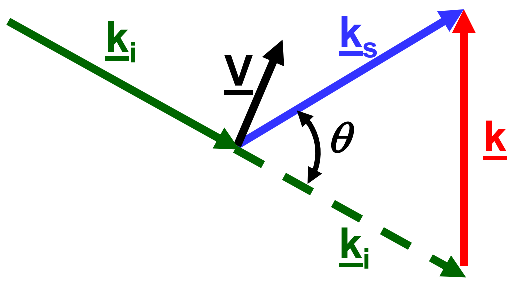

$$|k_s| \approx |k_i|$$

$$|k| = 2\frac{\omega_i}{c} sin(\frac{\theta}{2}) = 2|k_i|\, sin(\frac{\theta}{2})$$

k_i, k_s are wave-vectors of incident and scattered radiation

V is velocity vector of an electron

$$\hbar\vec{k}_i + m\vec{V} = \hbar\vec{k}_s + m(\vec{V} + \Delta\vec{V}) \qquad \textbf{momentum}$$

$$\hbar\omega_i + \frac{mV^2}{2} = \hbar\omega_s + \frac{m(\vec{V} + \Delta\vec{V})^2}{2} \qquad \textbf{energy}$$

$$\Downarrow$$

$$\omega_s - \omega_i = \vec{V} \cdot (\vec{k}_s - \vec{k}_i) \equiv \vec{V} \cdot \vec{k}$$

Change in frequency is determined by the component of velocity || to vector <u>k</u>

Thomson scattering

Scattering by plasma

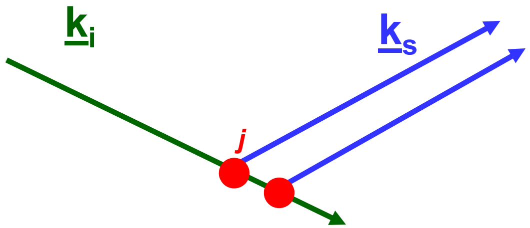

Total electric field in the scattered wave is the sum of electric fields scattered from a large number of small plasma cells

(each with density $n_e = n_e + \delta n_e$ and phase shift φ_j)

$$E_s \sim \sum_j (\langle n_e \rangle + \delta n_e) exp(-i\phi_j) \sim \sum_j \delta n_e \, exp(-i\phi_j) \qquad \left(\langle n_e \rangle \sum_j exp(-i\phi_j) = 0 \right)$$

(no scattering from uniform media)

$$I_s \sim \langle E_s E_s^* \rangle \sim \sum_{jk} \langle \delta n_k \delta n_j \rangle \, exp\left(-i(\phi_k - \phi_j)\right) \Rightarrow$$

Scattering signal is determined by correlation of density fluctuations in plasma

Plasma quasi-neutrality (Debye shielding):

$D < \lambda_D$ – density fluctuations from thermal motion

$D > \lambda_D$ – from collective modes (waves)

Scattering parameter

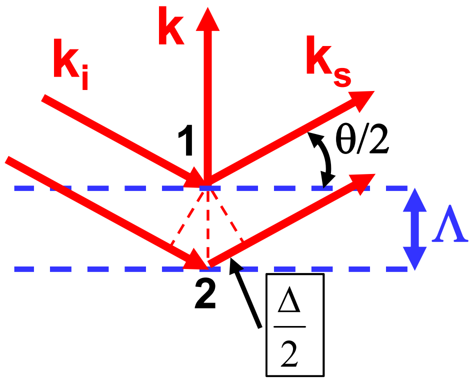

waves scattered from two cells (1 and 2), separated by distance Λ along scattering k-vector, have a path difference Δ :

$$\Delta = 2\Lambda\, sin(\frac{\theta}{2}) = \lambda_i \quad for \quad \Lambda = \frac{2\pi}{k} \quad with \quad k = 2k_i\, sin(\frac{\theta}{2})$$

$$\boxed{compare\ \Lambda\ with\ \lambda_D \Rightarrow scattering\ parameter\ \alpha}$$

$$\alpha \equiv \frac{1}{k\lambda_D} = \frac{\lambda_i}{4\pi\lambda_D\, sin(\theta/2)} \qquad \alpha = \frac{1.08\cdot 10^{-4}\,\lambda_{[cm]}}{sin(\theta/2)}\left(\frac{n_{e[cm^{-3}]}}{T_{e[eV]}}\right)^{1/2}$$

α<<1 ($\Lambda << \lambda_D$) => **scattering on fluctuations occurring on spatial scales << λ_D , thermal fluctuations inside Debye sphere (incoherent scattering)**

α>>1 ($\Lambda >> \lambda_D$) => **scattering on collective modes, from electrons which motions are correlated (coherent scattering)**

Thomson scattering

Thomson scattering spectral density function

$$\sigma = \sigma_T \cdot S\left(\vec{k}, \omega\right) \qquad (\omega \equiv \omega_s - \omega_i)$$
$$S(\vec{k}, \omega) = S_e(\vec{k}, \omega) + S_i(\vec{k}, \omega)$$

[Froula *et al*. "Plasma scattering of electromagnetic radiation", 2010]

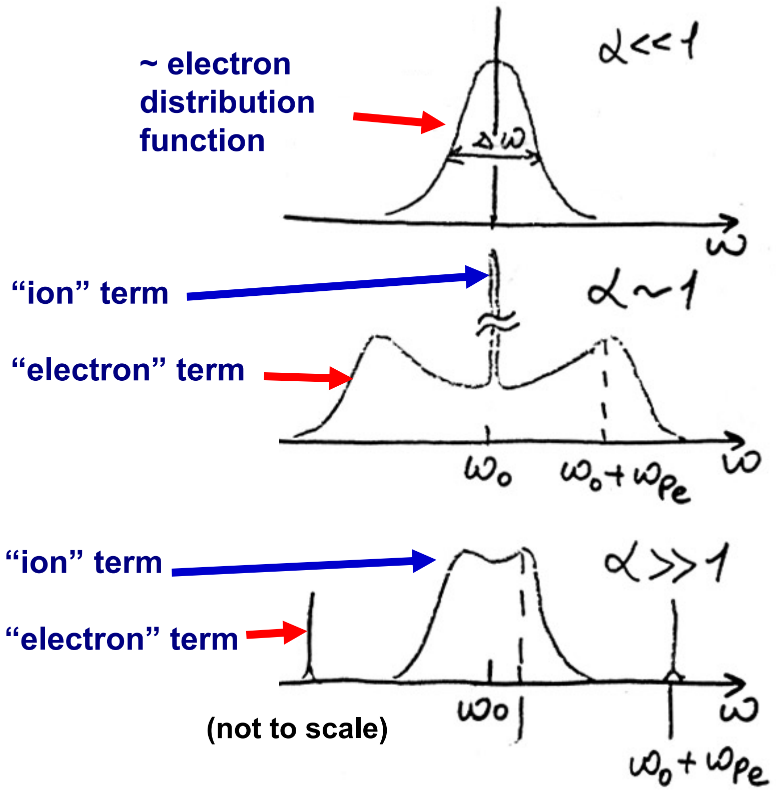

Qualitatively:

"Ion" and "electron" terms in the total scattering -

EM are scattered by the electrons (ions are too heavy)!

Debye shielding in plasma

Electron motions are followed by "electron cloud" (+e):

Fast motions, large frequency shifts, "electron" term

Ion motions shielded by electron cloud (-e/2) and by "ion cloud" (-e/2)

Slow motions, small frequency shifts, "ion" term

Thomson scattering

$$\boxed{\alpha = \frac{1}{k\lambda_D} << 1} \longrightarrow$$

Incoherent scattering: fluctuations are determined by thermal motion of electrons

(low density, high temperature, large scattering angles)

$$S_e(k,\omega) = \int f(\vec{V})\delta(\omega - \vec{k}\vec{V})d\vec{V}$$

- f(V) is the electron distribution function

$$S_e = n_e\sqrt{\frac{m_e}{2\pi T_e k^2}}\, exp\left(-\frac{m_e\omega^2}{2T_e k^2}\right)$$

- for Maxwellian distribution

$$\frac{\Delta\lambda_{1/2}}{\lambda} = 6.6\cdot 10^{-3}\sqrt{T_{e[eV]}}\, sin(\theta/2)$$

e.g., $\Delta\lambda$ = 25nm for Nd laser (532nm) at 90^0 (for plasma with T_e=100eV)

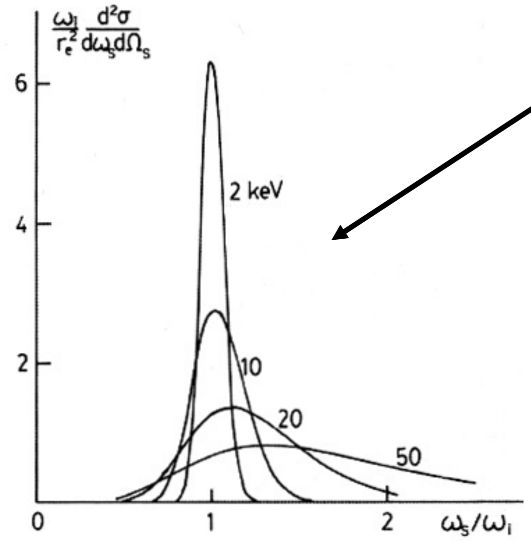

Relativistic effects at high T

Possibility to measure electron distribution function (e.g. presence of fast electrons)

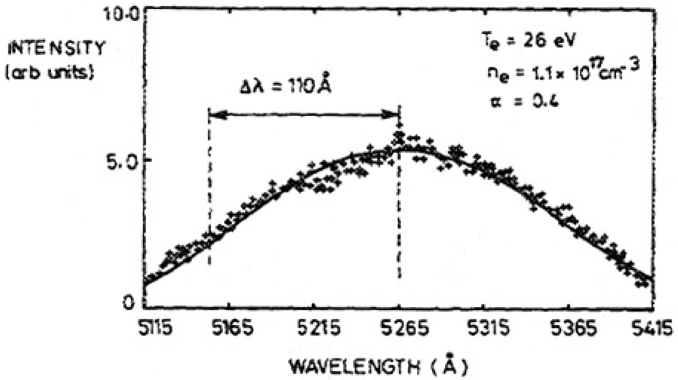

Thomson scattering

$$\boxed{\alpha = \frac{1}{k\lambda_D} \geq 1} \rightarrow$$

Coherent scattering:

scattering from test electron is balanced by scattering from the shielding (electron) cloud $\Rightarrow S_e \Rightarrow 0$

for a test ion scattering is from the shielding electron cloud $\Rightarrow S_i$ dominates ("scattering on ions")

(high density, low temperature, small scattering angles)

Total scattering (frequency integrated)

$$S_e = \frac{1}{1+\alpha^2}$$

$$S_i \approx \frac{Z\alpha^4}{(1+\alpha^2)\left(1+\alpha^2+(ZT_e/T_i)\alpha^2\right)}$$

$$\Delta\omega_i \sim k\sqrt{\frac{T_i}{M_i}} << \Delta\omega_e$$

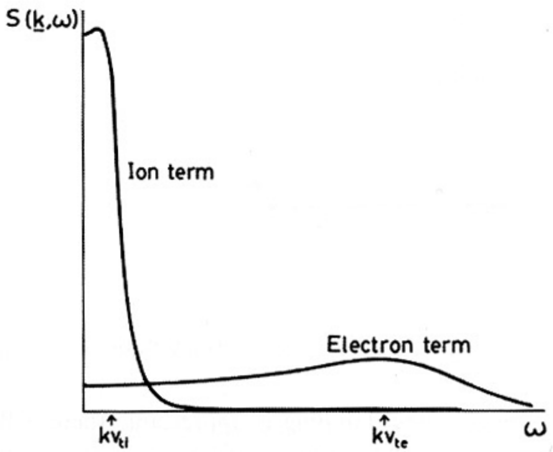

A. Dangor et al, JAP v.64 (1988)

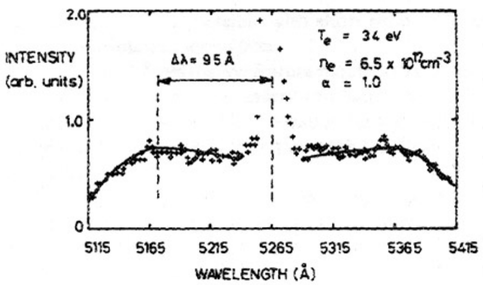

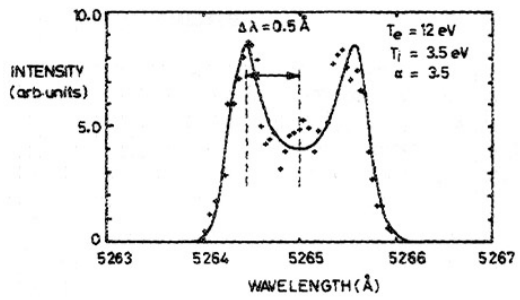

Narrow ion feature centred on broad electron spectrum. Electron peaks give plasma density:

$$(\Delta\omega)^2 = \omega_p^2(1+3/\alpha^2)$$

Ion wings due to ion acoustic resonance

$$\Delta\omega = k\left(\frac{\alpha^2}{1+\alpha^2}\frac{k_B T_e}{m_i} + \frac{3k_B T_i}{m_i}\right)^{1/2}$$

s.lebedev@ic.ac.uk May 2019

Thomson scattering

Experimental considerations

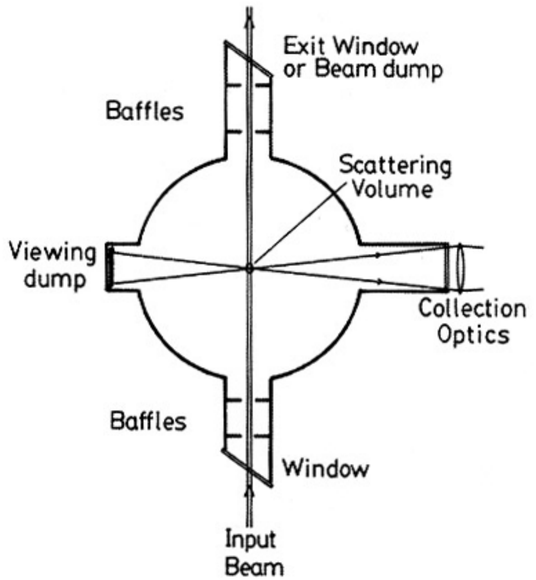

Need to suppress scattering from the walls, windows and optics

or separate by time-of-flight for short laser pulses

Amplitude of the signal (lower limit on density)

$$\frac{P_S}{P_{Laser}} \sim n_e \sigma_T L \Delta\Omega \quad \sim 10^{-10} \; for\; n_e \sim 10^{18}\, cm^{-3}$$

Plasma light (upper limit on density)

$$P_S \propto n_e \qquad\qquad P_{ff,fb} \propto n_e^2$$

Scattering geometry – plasma light is collected from a larger volume than scattered

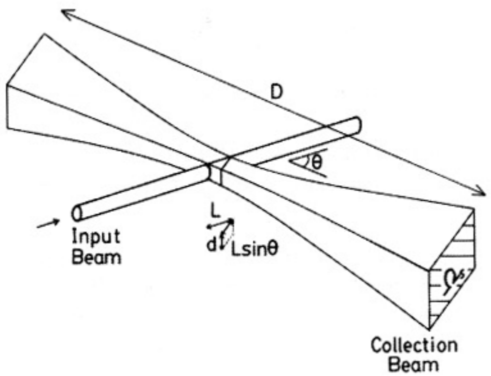

s.lebedev@ic.ac.uk May 2019

Thomson scattering

Experimental considerations

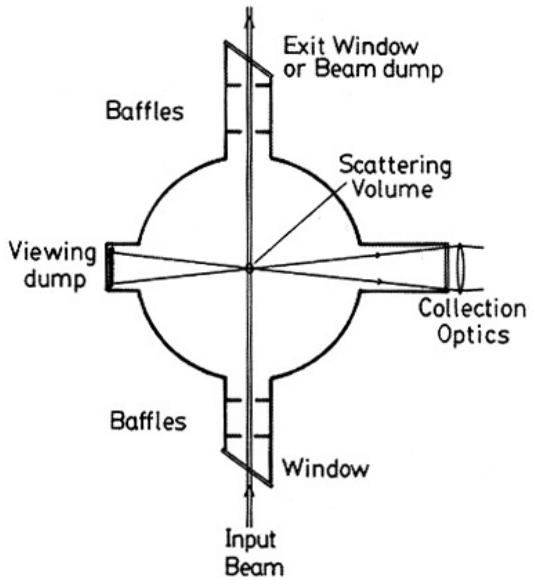

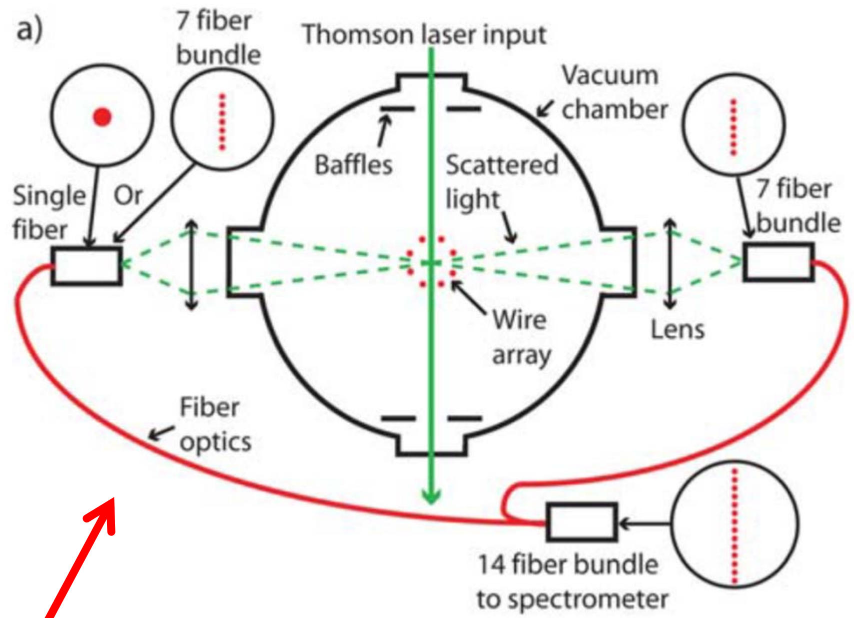

Spatially resolved scattering using fibre-optics and imaging spectrometer

Measurements of plasma flow velocity and plasma temperature

(MAGPIE facility at Imperial College)

[Harvey-Thompson *et al.*, PRL 2012 & PoP 2012]

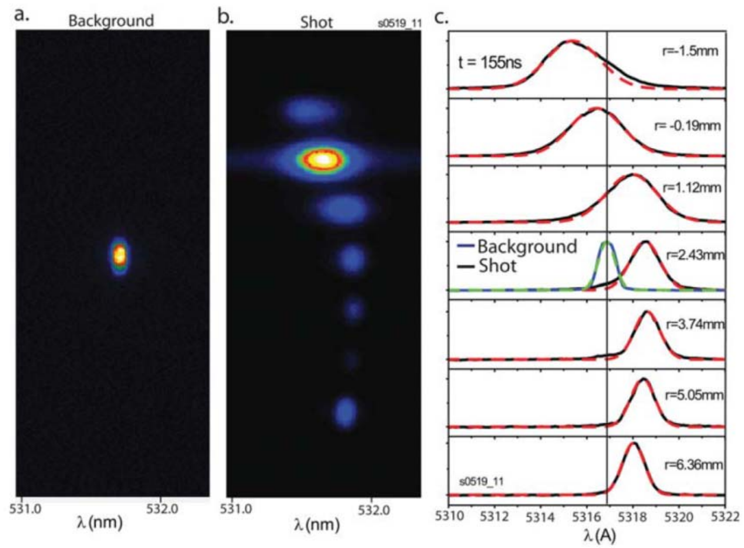

Outline

Electrical measurements: magnetic field and current

Laser probing: interferometry, density gradients

Emission: spectral lines, continuum

Thomson scattering

X-ray imaging

Proton probing

X-ray imaging

Pin-hole camera

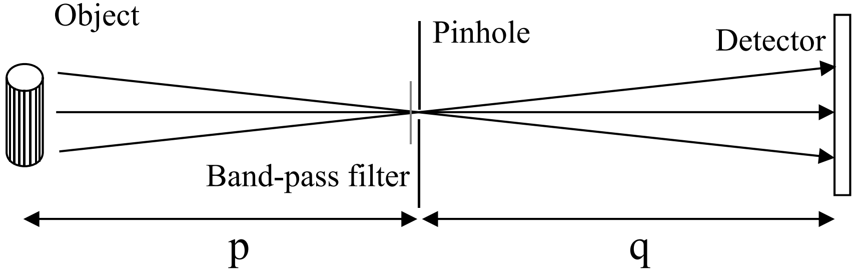

Magnification $$M = \frac{q}{p}$$

Geometrical resolution
(Δ is pin-hole size)

$$\delta = \Delta\left(\frac{M+1}{M}\right)$$

"Diffraction" resolution

$$\delta_d = 1.22\frac{\lambda q}{\Delta}\cdot\frac{1}{M}$$

Imploding Z-pinch

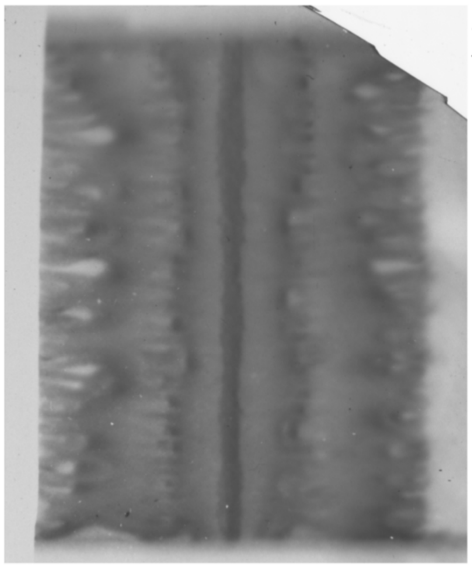

Detector:

X-ray film (time-integrated) or MCP camera (time-resolved)

Detector irradiation: $$\frac{energy}{unit\ area} \propto \frac{\Delta^2}{q^2}$$

X-ray radiography

Point-projection

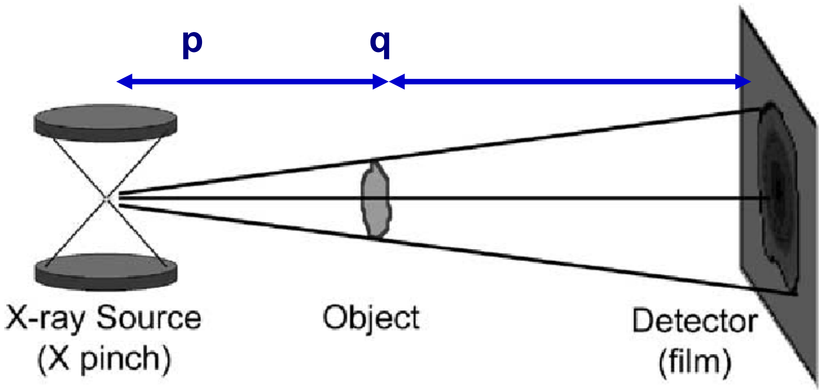

Magnification $$M = \frac{q+p}{p}$$

Geometrical resolution $$\delta = \sigma \cdot \left(\frac{M-1}{M} \right)$$

(σ is the source size)

Detector: film (time-integrated) or MCP

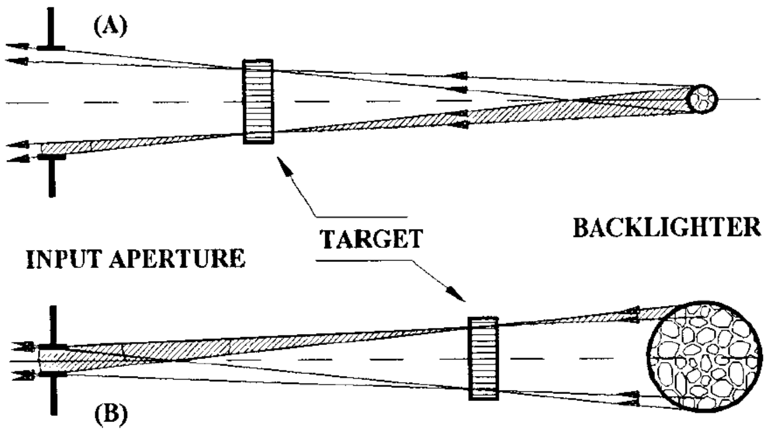

Point-source backlighter

Area backlighter (requires high uniformity)

s.lebedev@ic.ac.uk May 2019

X-ray spectroscopy and radiography with spherical crystals

Radiography

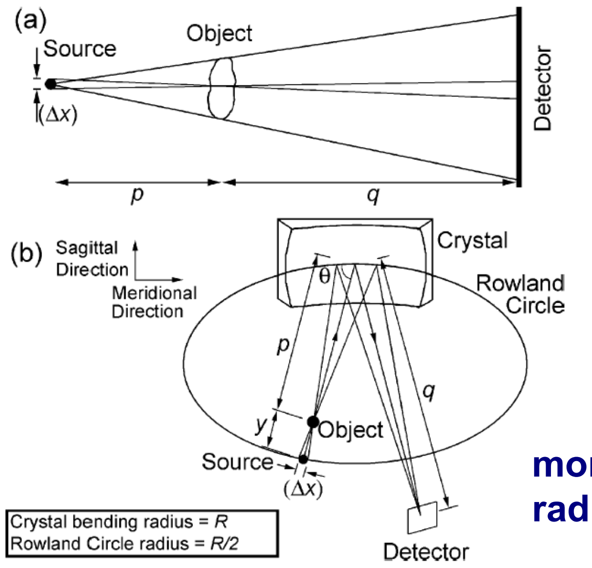

monochromatic radiography

Plasma jet and imploding capsule on Z

D. Sinars et al., RSI, v.75 (2004)

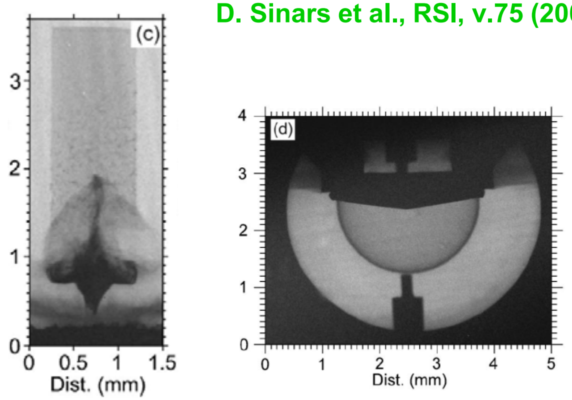

Spectroscopy with 1D spatial resolution

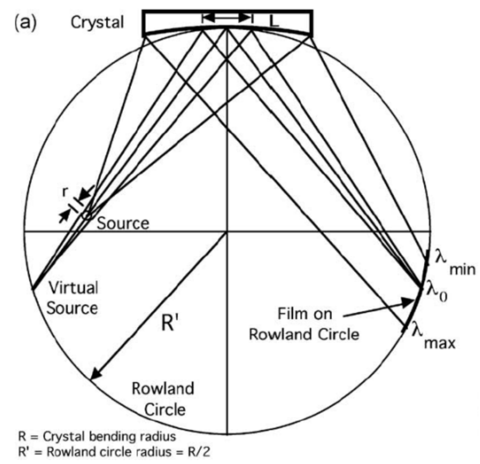

Spectrum of Al Z-pinch on Magpie

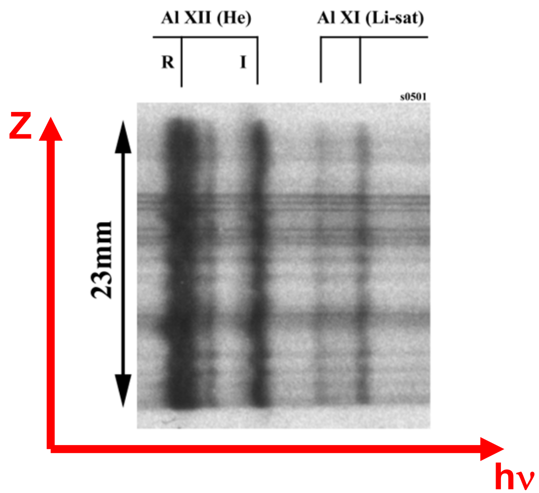

s.lebedev@ic.ac.uk May 2019

Probing with ion beams

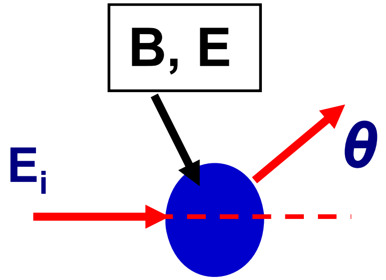

Deflection of ions by electric or magnetic fields

For small angles:

$$\boxed{\sin(\theta) = \frac{q}{\sqrt{2m_i E_i}} \cdot \int B \times dl \approx 7 \cdot \frac{\int B \times dl[T \cdot m]}{\sqrt{A \cdot E[MeV]}}}$$

$$\boxed{\tan(\theta) = \frac{q}{2E_i} \cdot \int E_\perp dl \approx \frac{1}{2E_i[MeV]} \cdot \int E_\perp dl\ [MV/m \cdot m]}$$

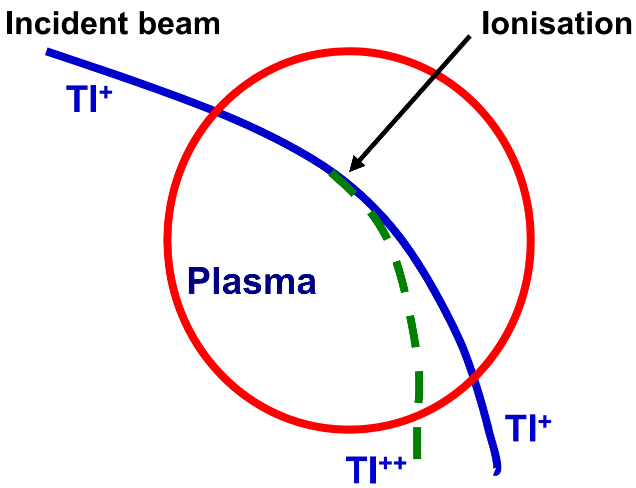

MCF: probing by heavy ions (A=200, E~300keV)

Measurements of electric potential in plasma:

- **position of ionisation from trajectory**
- **potential from change of energy**

Proton probing

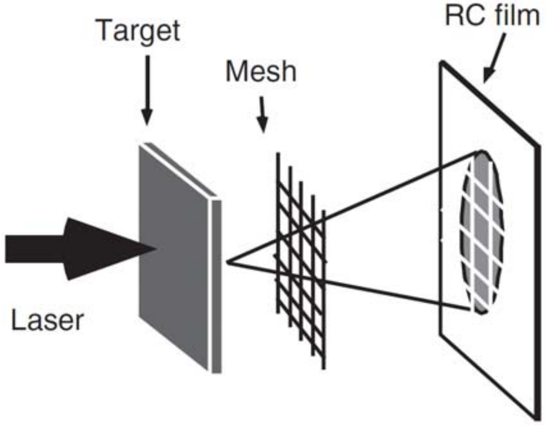

Proton beam from laser irradiated foil (~MeV with broad energy spectrum)

Registration on stack of radiohromic films, to provide energy resolution

- **Point-projection imaging with MeV energy protons**
- **Proton attenuation is typically negligible, deflection by E- and B-fields**
- **Broad energy spectrum of protons.**
- **Different layers in the film stack correspond to different proton energy – can be used for time-resolved imaging (ps time-of-flight delay)**

Proton probing

Macchi *et al.*, RMP, v.85 (2013)

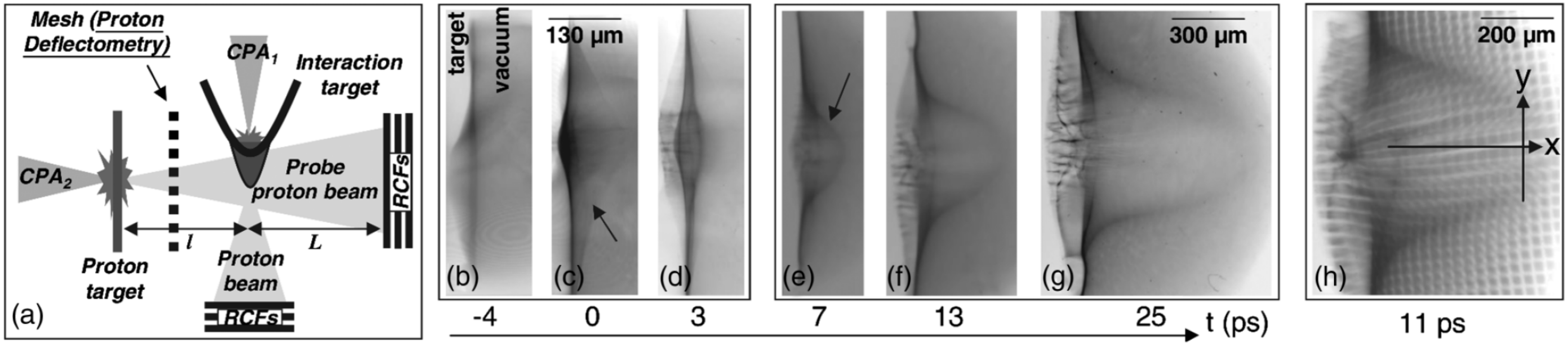

- **Point-projection imaging with MeV energy protons**
- **Proton attenuation is typically negligible, deflection by E- and B-fields**
- **Broad energy spectrum of protons.**
- **Different layers in the film stack correspond to different proton energy – can be used for time-resolved imaging (ps time-of-flight delay)**

Proton probing

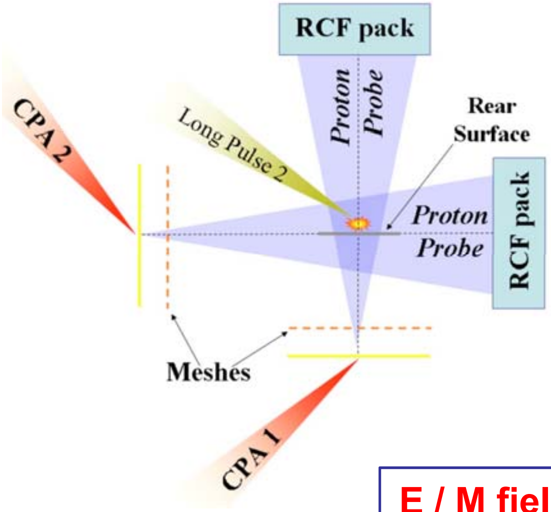

Proton beam from laser irradiated foil (broad energy spectrum)

Registration on stack of radiohromic films, to provide energy resolution

Cecchetti et al., Phys. Plas. v.16 (2009)

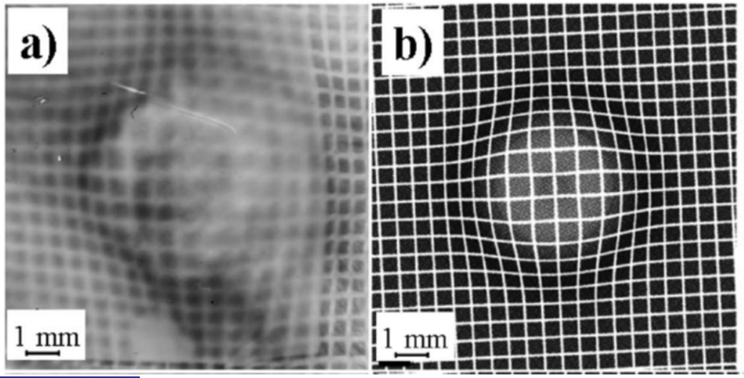

E / M fields: Kugland et al., RSI 83, 101301 (2012)

Rygg, et al., Science v.319 (2008)

15MeV D^3He fusion protons (mono-energetic)

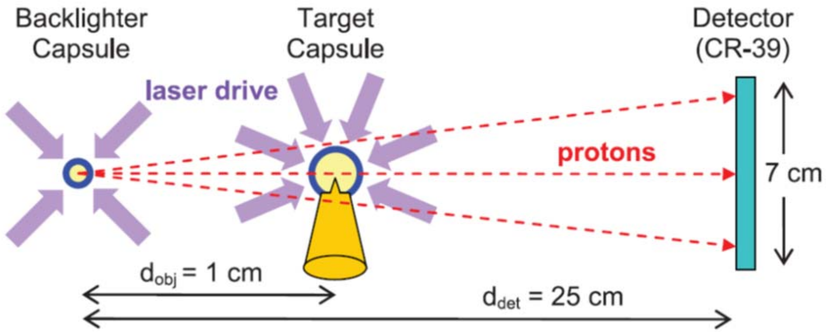

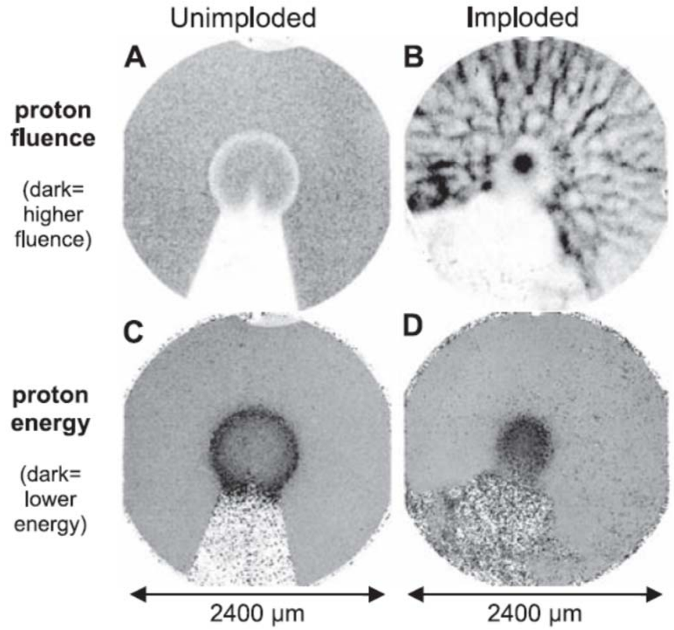

Bibliography

Books

“Principles of plasma diagnostics”, I.H. Hutchinson

“Laser-aided diagnostics of plasmas and gases”, K. Muraoka, M. Maeda

“Plasma diagnostics”, W. Lochte-Holtgreven

“Plasma diagnostic techniques”, R.H. Huddlestone & S.I. Leonard

“Plasma scattering of electromagnetic radiation”, D.H. Froula, S.H. Glenzer, N.C. Luhmann, J. Sheffield (2010)

Review articles

“Instrumentation of magnetically confined fusion plasma diagnostics”, N.C. Luthmann & W.A. Peebles, Rev. Sci. Instruments, v.55, 279 (1984)

“Diagnostics for fusion reactor conditions”, E. Sindoni & C. Warton, eds. (Varenna School on plasma physics, 1978)

Proceedings of conferences “High Temperature Plasma Diagnostics”, published in journal Rev. Sci. Instruments (every two years), include review articles on the present state of different diagnostic techniques